ADVANCED ENGINEERING MATERIALS



DOI: 10.1002/adem.201200231

# Design, Processing, Microstructure, Properties, and Applications of Advanced Intermetallic TiAl Alloys**

By *Helmut Clemens* and *Svea Mayer**

*After almost three decades of intensive fundamental research and development activities, intermetallic titanium aluminides based on the ordered γ-TiAl phase have found applications in automotive and aircraft engine industry. The advantages of this class of innovative high-temperature materials are their low density and their good strength and creep properties up to 750 °C as well as their good oxidation and burn resistance. Advanced TiAl alloys are complex multi-phase alloys which can be processed by ingot or powder metallurgy as well as precision casting methods. Each process leads to specific microstructures which can be altered and optimized by thermo-mechanical processing and/or subsequent heat treatments. The background of these heat treatments is at least twofold, i.e., concurrent increase of ductility at room temperature and creep strength at elevated temperature. This review gives a general survey of engineering γ-TiAl based alloys, but concentrates on β-solidifying γ-TiAl based alloys which show excellent hot-workability and balanced mechanical properties when subjected to adapted heat treatments. The content of this paper comprises alloy design strategies, progress in processing, evolution of microstructure, mechanical properties as well as application-oriented aspects, but also shows how sophisticated ex situ and in situ methods can be employed to establish phase diagrams and to investigate the evolution of the micro- and nanostructure during hot-working and subsequent heat treatments.*

## 1. Introduction

New structural materials have to be ''stronger and lighter'' to withstand the extremely high demanding conditions in the next generation of automotive and aircraft engines, which are targeted to exhibit higher efficiency leading to reduced fuel consumption as well as significantly decreased $CO_2$ emissions. Intermetallic γ-TiAl based alloys possess numerous

[*] *Prof. H. Clemens, Dr. S. Mayer*
*Department of Physical Metallurgy and Materials Testing, Montanuniversitaet Leoben, 8700 Leoben, Austria*
*E-mail: helmut.clemens@unileoben.ac.at*

[**] *A part of the work presented in this review paper was conducted within the framework of the following projects: FWF project P20709-N20, Austria; COMET Competence Centre Programme, Austria; FFG project 826989 ''ProStTial'', Austria; FFG project 832040 ''energy-drive,'' Research Studios Austria, Austria; FFG project 830381 ''fAusT,'' Österreichisches Luftfahrtprogramm TAKE OFF, Austria; Styrian Materials Cluster, Austria; BMBF project O3X3530A, Germany. The support of the DESY and ESRF managements and user offices is gratefully acknowledged. We appreciate the commitment of the HZG and ESRF beam-line staff which contributed greatly to the success of the experiments performed. Research activities performed at DESY have received funding from the European Community's Seventh Framework Programme (FP7/2007-2013) under grant agreement no. 226716. Finally, we thank our project partners for many years of fruitful cooperation and our PhD students who are working in the framework of the programs listed above: Thomas Schmoelzer, Martin Schloffer, Emanuel Schwaighofer, Robert Werner, and Andrea Gaitzenauer.*
*This paper was amended in issue 4 of Advanced Engineering Materials because there was a mistake in the Early View publication.*

  

attractive properties which meet these demands and they also represent a good example how fundamental and applied research along with industrial development can lead to a new class of advanced engineering materials.[1–12] The intention of this review is to give a short summary of a dynamic field of materials research which became even more accelerated by the trend-setting step of General Electric, who equipped the last stage(s) of the low-pressure turbine (LPT) of the so-called GEnX jet engine with cast TiAl blades.[13] Additionally, the automotive industry is eager to establish TiAl as innovative structural materials, e.g., for the use as turbocharger turbine wheels in their drive system to meet the future environmental requirements claimed by legislative authorities. Although the present paper deals mainly with results achieved by the authors in the framework of European as well as international collaborations with universities, research facilities, and industries, additional reference to other world-wide activities is given. This paper provides an overview, for specific information the reader will be referred to recent papers, review articles, conference and workshop proceedings, and textbooks which focus on all aspects of alloy development, deformation mechanisms, microstructural evolution, processing, and machining as well as component tests and applications. Especially the conference and workshop proceedings which comprise almost 25 years of research and development prove how TiAl alloys matured from laboratory ''curiosities'' to novel structural light-weight materials which eventually found their applications.

Due to their attractive properties, intermetallic γ-TiAl based alloys are considered for high-temperature applications in aerospace and automotive industries.[2,9,12,14–23] Their advantage is mainly seen in low density (3.9–4.2 g cm$^{-3}$, depending on composition and constitution), high specific yield strength, high specific stiffness, good oxidation resistance, resistance against ''titanium fire,'' and good creep properties up to high temperatures. The variation of the specific yield strength and the specific elastic modulus with temperature of various γ-TiAl based alloys in comparison with Ni-base superalloys and Ti-base alloys is shown in Figure 1a and b.[24] In addition, the thermo-physical properties, also in comparison with conventional materials, are summarized in Figure 2. Particularly at temperatures between 600 and 800 °C γ-TiAl based alloys are superior to Ti-alloys in terms of their specific strength. Compared to the heavier Ni-base alloys, their specific strength is at least similar. In the last years, novel high-strength γ-TiAl based alloys, such as TNM$^{TM}$ alloys,[25,26] have been developed which define the upper strength limit of the advanced titanium aluminides in Figure 1. These alloys are characterized by a high content of β-stabilizing alloying elements, such as Nb and Mo. Since Nb and Mo represent the decisive alloying elements, this alloy family, based on the γ-TiAl phase, has been named ''TNM alloys'' in order to distinguish them from the well-known and even stronger ''TNB alloys'' which rely on a high Nb concentration and small additions of B and C.[11,12] At room temperature strength levels >1000 MPa can be achieved in

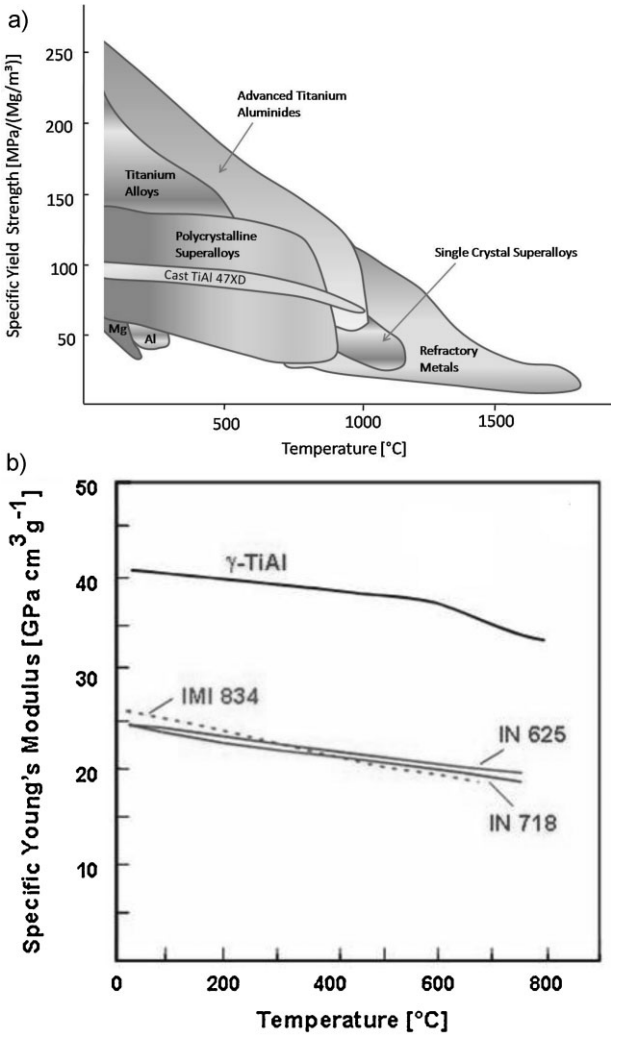


*Fig. 1. Variation of (a) specific yield strength and (b) specific Young's (elastic) modulus with temperature of selected structural materials in comparison with intermetallic γ-TiAl based alloys.[2,24] The upper strength limit of the advanced titanium aluminides represents data obtained on forged and heat treated TNM$^{TM}$ alloys.*

advanced TiAl alloys by appropriate thermo-mechanical processing and subsequent heat treatments. It is important to note that also high temperature properties, such as creep resistance, were considerably improved, e.g., by implementation of precipitation hardening, which further extend the application range of γ-TiAl based alloys.

In general, advanced TiAl alloys such as TNB and TNM alloys are complex multi-phase alloys which can be processed by ingot or powder metallurgy as well as precision casting methods.[6,7,9,12,27] Each process leads to specific microstructures which can be altered and optimized by thermo-mechanical processing and/or subsequent heat treatments.[7,12,28] In order to further increase the economic feasibility of wrought processing for manufacturing of γ-TiAl components, alloys are needed which can be hot-forged under isothermal conditions, but also near-conventional, which, e.g., means that a conventional forging equipment with minor and inexpensive modifications can be used.[26,29] The background

  

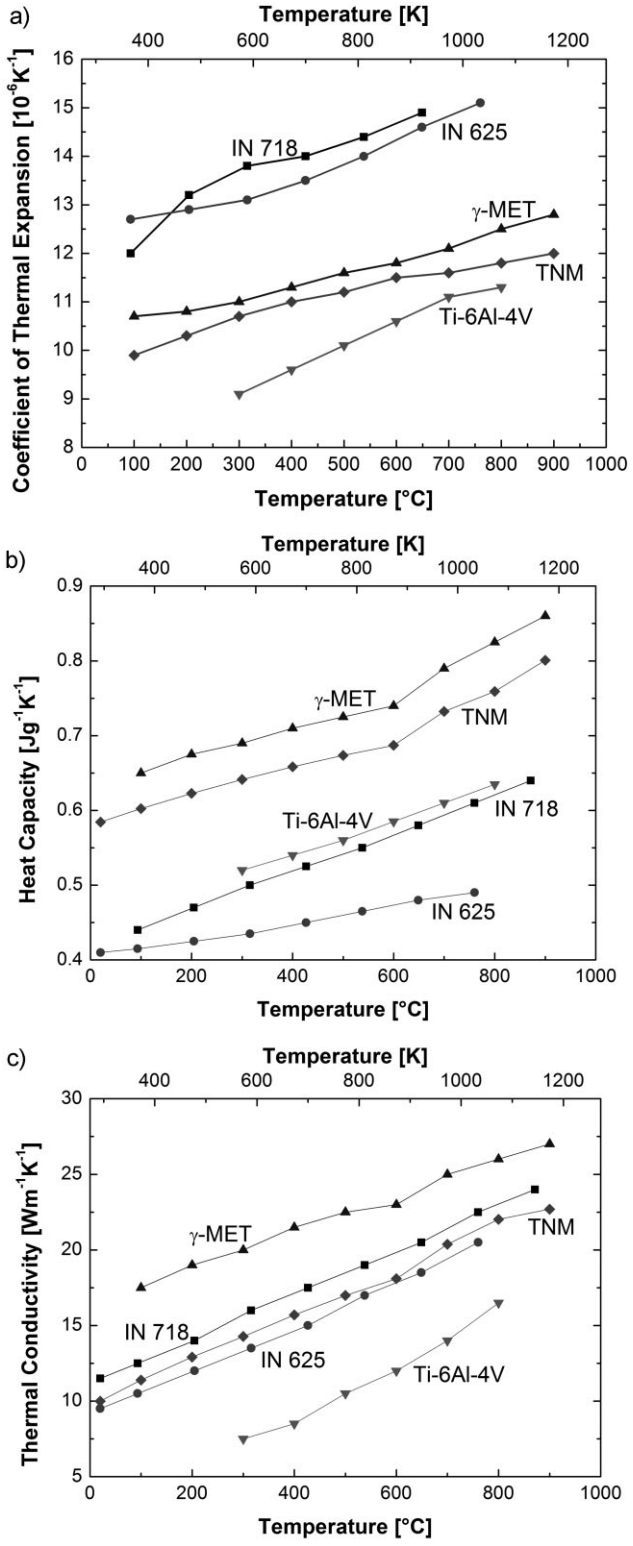


*Fig. 2. Thermo-physical properties as a function of temperature of a TNM™ alloy in comparison with Ti-base alloys and superalloys. The alloy termed γ-MET represents a typical 2nd generation γ-TiAl based alloy with the composition Ti–46.5Al–4(Cr, Nb, Ta, B).[2] (a) coefficient of thermal expansion; (b) heat capacity; (c) thermal conductivity.*

of conducting heat treatments is manifold, i.e., to acquire chemical and microstructural homogeneity as well as to increase both the ductility at room temperature and creep strength at elevated temperature. In order to achieve this goal, the knowledge of the occurring solidification processes along with the following phase transformation sequences is essential. Therefore, thermodynamic calculations are helpful to predict the phase diagram of engineering TiAl alloys. After verification with experimental methods, e.g., short and long-term heat treatments combined with quantitative metallography, differential scanning calorimetry (DSC), conventional X-ray diffraction (XRD) and in situ high-energy X-ray diffraction (HEXRD), these phase diagrams provide the basis for the development of effective heat treatments. To account for the influence of deformation and kinetic aspects sophisticated ex situ and in situ methods have been employed to investigate the evolution of both microstructure and texture during thermo-mechanical processing and subsequent multiple heat treatments.[30] For example, HEXRD was conducted to study dynamic recovery and recrystallization processes in TNM alloys during hot-compression testing.[31,32] While XRD diffraction gives high intensities for the main reflections of the occurring phases, ordering phenomena are difficult to detect. Due to the peculiar scattering behavior of TiAl alloys neutron diffraction gives high intensities for the superstructure peaks of ordered phases, while the intensities of the main peaks are very small.[30,33,34] Consequently, in situ neutron diffraction experiments were employed to determine the ordering temperature of the $\alpha_2$- and $\beta_o$-phase in the TiAl–Mo and TiAl–Nb–Mo systems.[30,35–37] Summarizing all results a consistent picture regarding microstructure formation and its impact on mechanical properties in advanced TiAl alloys can be given.

In 1999, the first commercial application of γ-TiAl based alloys was announced. Mitsubishi has implemented TiAl turbocharger wheels in their Lancer Evolution 6 sports car.[18] In 2002, the serial production of wrought processed high-performance γ-TiAl valves for racing car application has started.[10,38] Only few years ago, an US aero engine manufacturer announced the initiation of investment cast γ-TiAl blades in the LPT.[13] Certification and flight tests with TiAl equipped engines have been conducted successfully and in the meantime the regular service for passenger transportation and carriage of freight has begun already.[39] This achievement has put pressure on all other major aircraft engine manufactures, which, in turn, have also announced the future use of TiAl.

## 2. Constitution and Properties of γ-TiAl Based Alloys

In order to understand the evolution of the micro- and nanostructure in intermetallic titanium aluminides and their impact on thermo-physical, chemical, and mechanical properties, in this chapter the constitution of γ-TiAl based alloys as well as current alloy design concepts for β-solidifying alloys, such as TNM alloys, will be reviewed comprehensively. Engineering γ-TiAl based alloys consist of γ-TiAl (ordered face – centered tetragonal $L1_0$ structure) and $\alpha_2$-$Ti_3Al$ (ordered

  

hexagonal $D0_{19}$ structure). The unit cell of the stoichiometric γ-TiAl phase is only slightly distorted ($c/a \approx 1.02$) and consists of alternating planes of Ti and Al atoms in the [001] direction.[40] In thermodynamic equilibrium, the $\alpha_2$-$Ti_3Al$ volume fraction is controlled by the Al-content and additional alloying elements which in total are typically in the range of 5–20 at%. However, thermo-mechanical processing and heat treatments have a strong influence on the actual $\gamma/\alpha_2$-volume fraction in γ-TiAl based alloys. In Al-lean alloys which contain additions of Cr, Nb, Mo, or W, a significant amount of β-TiAl phase with disordered body-centered cubic (bcc) structure or its ordered counterpart with B2 structure is often formed. Micro-alloying with C, B, and Si leads to the formation of various types of carbides, borides, and silicides, because the solubility limit of these elements in γ-TiAl and $\alpha_2$-$Ti_3Al$ phase is relatively low.[1,4,9,12,40]

Like in structural metallic materials the ductility and strength of intermetallic γ-TiAl based alloys are controlled by chemical composition and microstructure. For fine-grained binary TiAl alloys, the room temperature elongation to fracture varies with Al-content, exhibiting a maximum at the two-phase composition Ti–48Al.[12,40,41] Note that in this paper all compositions are stated in atomic percent, unless indicated otherwise. Since low-temperature ductility is a major concern for structural applications, γ-TiAl alloys of engineering importance are based on Ti–(42–48)Al.[2,12,40–43] However, even at the beginning of the development activities it was recognized that binary two-phase alloys can generally not be used due to their inability to meet requirements such as creep strength and resistance to oxidation. As a consequence, the effect of alloying elements on the mechanical properties of two-phase γ-TiAl based alloys with specific types of microstructure has been investigated within the framework of extensive research and development programs. The output of these programs was the definition of the compositional range of the so-called 1st and 2nd generation of TiAl alloys as summarized in ref.[40,42] Alloying additions, such as Cr, Mn, and V, in combination with thermo-mechanical processing led to further improvements, where a plastic fracture elongation up to 3% can be achieved at room temperature.[42,44–46] The occurring deformation mechanisms within the constituting phases at ambient and elevated temperatures have been content of numerous studies which findings remarkably influenced further alloy and processing development. For details regarding dislocation types and kinetics as well as activation parameters the reader is referred to the following references.[1,3,7,8,12,40,47] Exemplarily, Figure 3a shows a transmission electron microscope (TEM) image of a deformed γ-TiAl grain within a Ti–46.5Al–4(Cr, Nb, Ta, B) alloy exhibiting a near-gamma microstructure.[48] It is well established that below the brittle-to-ductile transition temperature, which depends on chemistry, microstructure, and test conditions (e.g., strain rate), the predominant deformation mechanisms in the γ-TiAl phase are the glide of ordinary $\frac{1}{2}<110]\{111\}$ dislocations and mechanical twinning along $\frac{1}{6}<11\bar{2}]\{111\}$. From Figure 3a it is evident, that in the

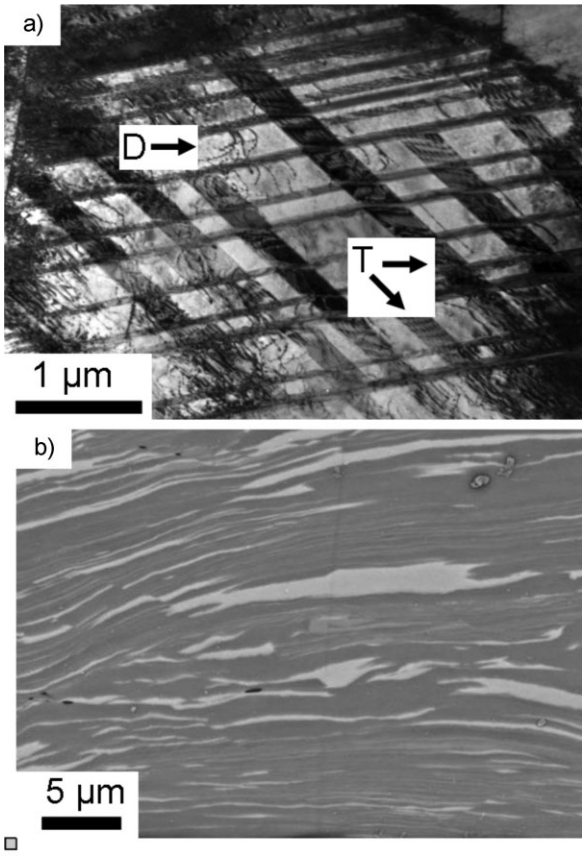


*Fig. 3. (a) TEM image of a Ti–46.5Al–4(Cr, Nb, Ta, B) sample deformed in compression up to 5% at room temperature reveals two different deformation mechanisms acting in γ-grains, deformation twinning (T) and dislocation glide (D). Note that cross-twinning with the primary twinning system limits the extension of the second twinning system;[48] (b) SEM image taken in back-scattered electron (BSE) mode of a Ti–43.5Al–4Nb–1Mo–0.1B alloy which was severely deformed at room temperature by means of high-pressure torsion to an equivalent strain of ≈3500%. The starting microstructure is shown Figure 16b.*

observed γ-TiAl grain more than one twin system has been activated. The onset of mechanical twinning during compression testing at room temperature was investigated in situ by means of acoustic emission measurements[48] and the obtained results were in good agreement with that gained from a theoretical model.[49] At this point it should be noted that also the conditions necessary for twin nucleation and growth have been treated theoretically by the group of Fischer *et al*.[50–54]

Due to the inherent brittleness of TiAl alloys their deformability at room temperature is limited even under compressive conditions. A method, however, which allows to study the influence of high strains is severe plastic deformation (SPD).[55] Figure 3b shows a scanning electron microscope (SEM) image of a β-stabilized TNM alloy (see below and Section 2.1) which was deformed at room temperature to an equivalent strain of ≈3500% by high-pressure torsion.[56] By means of such experiments, e.g., it is possible to study deformation-induced disordering phenomena at ambient temperatures in multi-phase TiAl alloys as recently demonstrated for an intermetallic FeAl alloy.[57]

  

ADVANCED ENGINEERING MATERIALS



The composition of 2nd generation γ-TiAl based alloys can be summarized as follows:

$$\text{Ti-(45-48)Al-(1-3)X-(2-5)Y-(}<1\text{)Z} \quad (1)$$

where X = Cr, Mn, V; Y = Nb, Ta, W, Mo; Z = Si, B, C.

Generally, the mentioned alloying elements alter the position of the phase boundaries of the Ti–Al-phase diagram. The stability between α and $\alpha_2$ as well as α ($\alpha_2$) and β-phases by additions of β-stabilizing elements was comprehensively investigated by ref.[58–62] For example, Nb and Mo as strong β-stabilizing elements shift the α-transus line to the Al-rich side, thus narrowing the $(\alpha+\gamma)$ phase field. For a fixed Al content this leads to an increase of the α (and $\alpha_2$) volume fraction. This effect is exploited in high Nb and Mo containing alloys (3rd generation TiAl alloys) where a significant refinement of the microstructure can be achieved.[11,26,63] Figure 4a shows a section of the binary Ti–Al-phase diagram in which the range of existence of γ-TiAl based alloys is marked by two vertically dotted lines. In case of binary alloys with an Al concentration below ≤45% solidification takes place via the β-phase, i.e., $L \rightarrow L+\beta \rightarrow \beta \rightarrow \ldots$, whereas a higher Al content leads to a peritectic solidification reaction, i.e., $L \rightarrow L+\beta \rightarrow \alpha+(\beta) \rightarrow \ldots$ Microstructural investigations by Küstner *et al.*[64] conducted on arc-melted binary alloy buttons have shown that Ti–45Al exhibits a microstructure consisting of large, equiaxed grains, whereas alloys with Al contents ≥47 at% clearly exhibited columnar grains which had grown in the direction of the heat extraction. The microstructural observations were supported by energy-dispersive X-ray (EDX) analysis where only small concentration fluctuations were observed in alloy Ti–45Al. These inhomogeneities might be attributed to the $\beta \rightarrow \alpha$ transformation or to segregation effects during solidification. Similarly, only modest concentration variations were found for the alloys Ti–45Al–5Nb, Ti–45Al–5Nb–1B and Ti–45Al–2Mo. In comparison, an alloy button with a composition of Ti–48Al exhibited strong fluctuations of Ti and Al, which indicate segregation due to dendritic solidification. Thus, from microstructural and microchemical investigations, it was concluded that all alloys on the base Ti–45Al solidified completely through the β-phase without pronounced segregation.[64] To study the solidification texture neutron diffraction was applied which, in contrast to XRD, allows examination of sample volumes of some cubic centimeters. For information regarding neutron diffraction on TiAl alloys in general and texture analysis in particular, the reader is referred to ref.[30,65] and ref.,[66–68] respectively. For example, Figure 5 shows the 110 pole figure of the γ-TiAl phase present in a cast Ti–43Al–4Nb–1Mo–0.1B ingot which solidified via the β-phase, e.g., $L \rightarrow L+\beta \rightarrow \beta$.[69] With a maximum pole density of 1.8 and a multiple random distribution (MRD), no statistically significant texture is prevailing after solidification and the subsequent solid phase transformations which occur during cooling to room temperature. In contrast, the inset in Figure 5 displays the 110 pole figure of a Ti–48Al alloy after peritectic solidification.[64] Here, a pronounced preferential

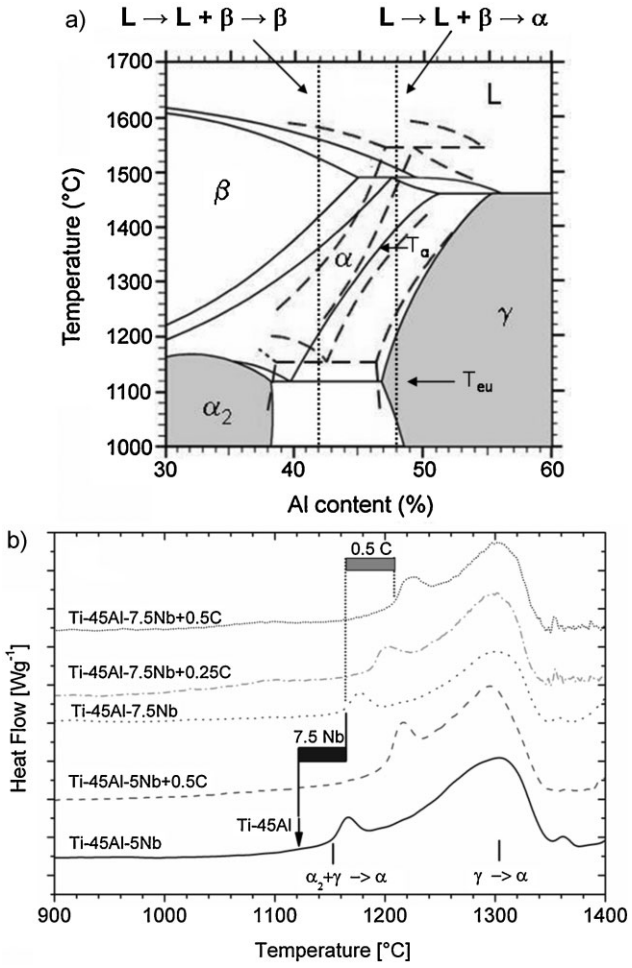


*Fig. 4. (a) Section of the binary Ti–Al-phase diagram (continuous lines). The range of the technical γ-TiAl based alloys is indicated by the two vertical dotted lines; $T_\alpha$: α-transus temperature; $T_{eu}$: eutectoid temperature. The broken lines show the effect of 8 at% Nb on the position of the phase field regions.[72] Nb stabilizes the β-phase and shifts the β-phase region to higher Al-contents. Concurrently, both melting point and eutectoid temperature are increased. The α-transus temperature ($\alpha+\gamma \rightarrow \alpha$), or alternatively termed γ-solvus temperature ($T_{\gamma,solv}$), which is important for processing these materials is lowered by the addition of Nb; (b) Effect of Nb and C additions on phase transformations in Ti–45Al.[73] The DSC curves were obtained from two ternary and three carbon containing alloys (see inset). A heating rate of 20 K min$^{-1}$ was used. For better readability the curves belonging to C-containing alloys were shifted along the ordinate. The arrow indicates the eutectoid temperature of binary Ti–45Al. The bars visualize the increase of $T_{eu}$ of the binary alloy evoked by alloying with 7.5 at% Nb and 0.5 at% C.*

orientation of the γ-grains is evident. The pole figure indicates that a preferential alignment of <110] directions perpendicular to the symmetry axis occurred. This texture corresponds with those usually observed for cast γ-TiAl alloys[70,71] and can be explained by a [0001] dendrite orientation of the hexagonal α-phase with respect to the heat flow direction. In conclusion, the microstructural observations of solidification of the β-stabilized Ti–43Al–4Nb–1Mo–0.1B alloy agree with the results of texture analysis as explained in detail in Section 4.1. The absence of an anisotropic casting texture, however, is beneficial as far as subsequent hot-forming operations are concerned.

  

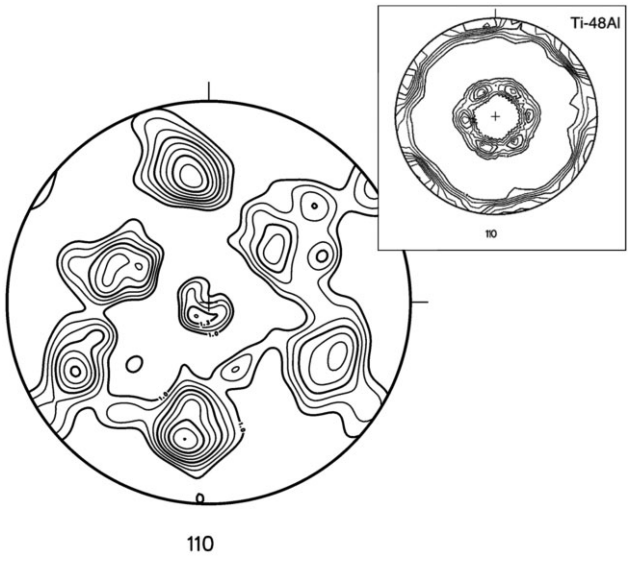


*Fig. 5. Recalculated 110 – pole figure of the γ-TiAl phase in alloy Ti–43Al–4Nb–1Mo–0.1B after casting and solidification. A maximum pole density of 1.8 MRD suggests no statistically significant texture. Inset: 110 – pole figure of an arc-melted Ti–48Al button (2.64 MRD). A well-developed casting texture is present (see text and ref.[69]).*

The broken lines in Figure 4a show the effect of 8% Nb on the position of the phase field regions according to Chen *et al*.[72] It can clearly be seen that Nb stabilizes the bcc β-phase and thus the β-phase field region is shifted to higher Al-contents. Additionally, the eutectoid temperature ($\alpha \rightarrow \alpha_2 + \gamma$) is increased significantly. The stabilizing effect of Nb and the change of the phase transformation temperatures by alloying with Nb can also be deduced from DSC measurements. The results of DSC measurements conducted on Nb and C containing Ti–45Al alloys are summarized in Figure 4b.[73] From Figure 4b it is evident that both, Nb and C, stabilize the $\alpha_2$-$Ti_3Al$-phase and thus raise the eutectoid temperature, whereas the α-transus temperature ($T_\alpha$), or equivalently, the γ-solvus temperature ($T_{\gamma,solv}$), of all alloys is almost identical. The alloying element Nb also lowers the stacking fault energy and thus increases the ductility of the alloys at room temperature by increasing the propensity for mechanical twinning.[12,74–76] In addition, Nb retards diffusion processes and modifies the structure of the oxidation layer.[77–79] The other alloying elements (Ta, W, and Mo) also improve the high temperature properties, like creep strength, by slowing down diffusion processes, but have a negative effect on oxidation resistance (Mo, W). Boron is typically used as a grain refining agent[12,42,80] and also influences the lamellar transformation in TiAl alloys.[81] Small additions of the silicide-forming element Si increase both the creep and oxidation resistance.[1,40–42] Carbon as an α-stabilizer widens the α-phase field region in the phase diagram. Additions of C also result in a reduction of the lamellar spacing within $\gamma/\alpha_2$-colonies which are formed upon cooling from the single α-phase field region.[82] The observed refinement of the lamellar microstructure is attributed to a segregation of C atoms to prior α grain boundaries which reduce the stacking fault energy and thus increase the frequency of fault formation. Since the faults enhance the heterogeneous nucleation of γ-TiAl at grain boundaries, C effectively increases the nucleation rate of γ-TiAl, thus resulting in a fine lamellar structure.[82] Likewise, upon ageing of supersaturated $\alpha_2$-$Ti_3Al$ grains of C containing TiAl alloys below the eutectoid temperature a significant refinement of the lamellar spacing within $\gamma/\alpha_2$-colonies is observed[83] which can be utilized to increase creep resistance. However, the important role of C in γ-TiAl based alloys with regard to precipitation hardening is discussed in the next paragraph.

According to Equation (1) engineering γ-TiAl based alloys of the 2nd generation contain at least one ''X''-element and one ''Y''-element to account for a good balance between ductility at room temperature and sufficient creep and oxidation resistance at elevated temperatures. An example of a 2nd generation alloy is Ti–48Al–2Nb–2Cr which was recently introduced as turbine blade material in jet engines.[13] However, like in the case of superalloys currently used, 2nd generation TiAl alloys may contain even more alloying elements, see ref.[2,10,40,42,43,47] Depending on alloy chemistry and microstructure, these alloys exhibit good workability, medium-to-good tensile properties (Figure 1), and tensile fracture strains in the range of 1–3% at room temperature as well as fracture toughness values ranging from 10 to 25 $MPa\sqrt{m}$.[40,42,47] The lower limit of the fracture toughness corresponds to fine-grained nearly gamma (NG) and duplex (D) microstructures, while the higher values are obtained for nearly lamellar (NL) and fully lamellar (FL) microstructures (see also Section 4). However, the creep resistance of these alloys seems to limit the maximum application temperature to 700 °C, especially if long-term service is considered. This is probably a direct consequence of thermally activated dislocation processes which make the mechanical behavior of γ-TiAl alloys strongly rate-dependent.[47] Thus, the strength degrades at low strain rates which normally occur under creep conditions. Additional limitations might arise from microstructural instabilities which are also expected to degrade the creep properties, and from an insufficient oxidation resistance at temperatures exceeding 700 °C.

In order to increase the high-temperature capabilities of γ-TiAl based alloys and, therefore, to widen the application range, alloy development programs were initiated which focused on high Nb and/or Mo containing alloys as well as precipitation hardened alloys, see ref.[2,5,8,10–12,17] For a large number of these 3rd generation alloys the constitution can be written as:

$$\text{Ti-(42-48)Al-(0-10)X-(0-3)Y-(0-1)Z-(0-0.5RE)} \quad (2)$$

where, X = Cr, Mn, Nb, Ta; Y = Mo, W, Hf, Zr; Z = C, B, Si. RE denotes rare earth elements.

The effects of alloying elements such as Hf, Zr, and RE elements on technological and mechanical properties have been studied in a variety of experimental TiAl alloys,[5,12,42,84–86] but they are not exploited in engineering alloys so far.

  

ADVANCED ENGINEERING MATERIALS



An example of advanced engineering γ-TiAl based alloys represent the so-called TNB alloys which exhibit Nb contents in the range of 5–10 at% and small additions of B and C. This class of high creep resistant alloys was developed at the Helmholtz Zentrum Geesthacht (formerly GKSS). Alloy development strategy, processing, microstructure evolution during hot-working and subsequent heat treatments as well as mechanical properties have been reported in numerous publications, e.g., see ref.[11,17,87–89] and a current textbook.[12] Another example of a 3rd generation alloy is the above-mentioned TNM$^{TM}$ alloy family which contains a balanced concentration of the β-stabilizers Nb and Mo. At elevated temperatures TNM alloys possess a large amount of disordered bcc β-phase which improves hot-workability. It was demonstrated that TNM alloys, in contrast to TNB alloys, can be forged using conventional forging equipment.[26,28] Post-forging heat treatments can be attuned to achieve moderate to near zero volume fraction of β-phase allowing a controlled adjustment of the mechanical properties.[28] The design philosophy of these β-solidifying alloys is described in Section 2.1. Both TNM and TNB alloys exhibit improved strength properties and oxidation resistance when compared with conventional 2nd generation TiAl alloys. For example, room temperature tensile strengths in the range of 800–1100 MPa were reported, along with plastic tensile strains >2%. The high contents of Nb and Mo impede diffusion processes, thus decreasing the climb rate of dislocations. Whereas this behavior is of advantage with regard to creep and thermal stability, the kinetics of phase transformations and recrystallization processes are slowed down. As a consequence the parameters of heat treatments and hot working operations must be adapted carefully.

Improvements in creep strength in 2nd and 3rd generation alloys have also been achieved by C additions in the range of 0.2–0.5 at%.[5,11,12,42,47,90] Annealing and quenching results in a C solid solution, whereas extremely fine precipitates are formed by subsequent ageing. TEM investigations conducted on binary TiAl-alloys with low additions of C have confirmed the presence of nanometer-sized acicular $Ti_3AlC$ precipitates of perovskite type which increased the strength properties considerably.[11,12,91,92] In case of Ti–45Al alloyed with 5 at% Nb and 0.5 at% C, also a significant strengthening effect was observed, but in spite of extensive TEM investigations no evidence of C containing precipitates was found.[88] Consequently, additional investigations were carried out employing atomic probe tomography (APT). Analysis of APT data revealed that by alloying with Nb, the limit of solubility of C in the γ-TiAl phase was increased significantly, thus suppressing the formation of precipitates.[89] The observed effect was attributed to the occurrence of Ti-antisite defects in the γ-TiAl phase which are formed due to the high Nb content. To explain this behavior, it should be kept in mind that in the γ-TiAl lattice Nb atoms exclusively substitute Ti lattice sites,[12,93] as revealed by atom location channeling-enhanced microanalysis (ALCHEMI)[94] and calculations using the discrete variational cluster method based on the local density approximation of the density functional theory.[95] Due to the presence of the Nb atoms in the Ti-rich γ-TiAl-phase, however, a fraction of Ti atoms is forced to occupy positions in the Al-sublattice, forming octahedral sites consisting of six Ti atoms (''$Ti_6$-type''). Such $Ti_6$-type sites exist in the $DO_{19}$ structure of the $\alpha_2$-$Ti_3Al$ phase which explains its high solubility for C atoms.[93] In contrast, the octahedral sites of the $L1_0$ structure of the γ-TiAl phase always possess a surrounding of mixed atom types, consisting of either four Al and two Ti atoms (''$Al_4Ti_2$-type'') or two Al and four Ti atoms (''$Al_2Ti_4$-type'') as shown in Figure 6a. This coordination seems to be unfavorable for C and O interstitials.[93,96] In the γ-TiAl phase of the investigated Ti–45Al–5Nb–0.5C alloy a solubility limit for C was determined, which was a factor of 10 higher than in binary alloys of comparable C-content which show the existence of $Ti_3AlC$-precipitates. In the Nb-containing alloy, however, C was found to be homogeneously distributed within the γ-TiAl-phase and the observed increase in strength was attributed to a solid solution strengthening effect.[89] Locally C enriched areas in the γ-TiAl-phase were found only at dislocations, forming so-called Cottrell atmospheres as shown in Figure 6b. However, in ref.[12,97] the existence of $Ti_3AlC$ precipitates in TNB alloys was evidenced by TEM. The inconsistency might be explained by differences in chemical composition, processing, and thermal history. In conclusion, precipitation-hardened γ-TiAl based alloys appear to be promising for

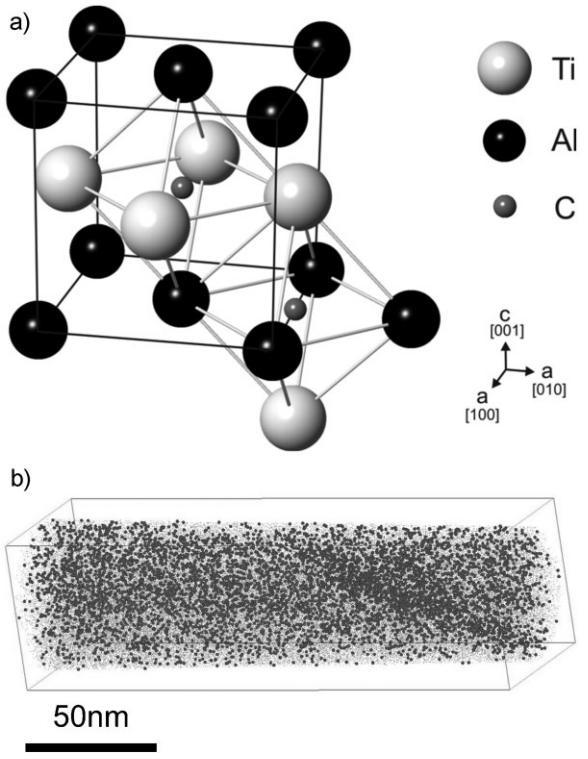


*Fig. 6. (a) Octahedral ''$Al_4Ti_2$-type'' and ''$Al_2Ti_4$-type'' cavities of the $L1_0$ structure of the γ-TiAl phase (after[93]); (b) C enrichment at a dislocation in the γ-TiAl-phase of a Ti–45Al–5Nb–0.5C alloy.[89] Every dot corresponds to a C atom. An Imago LEAP 3000XSi atomic probe was used for the investigation.*

  

high-temperature service. However, implementation of precipitation hardening often tends to embrittle the material, which is of particular concern in case of less ductile materials like γ-TiAl based alloys. However, it was reported for TNB alloys that adequate processing routes can lead to a homogeneous and relatively fine microstructure. For example, hot-extrusion resulted in well balanced mechanical properties which are characterized by a good creep resistance and an appreciable room temperature ductility of 2.5%.[11,12] In the meantime, so-called TNM$^+$ variants have been produced which contain harmonized additions of C. The C content was chosen to lie below the solubility limit of the γ-TiAl phase. As a consequence no precipitation reaction is occurring. First orienting creep tests have shown increased creep resistance when compared to C-free TNM alloys. Obviously, the proven strengthening effect can be attributed to a solid solution effect. Such an alloy system, however, is not prone to particle coarsening effects which might take place under creep conditions.[98] Besides perovskite phases, silicide or Laves phases may be attractive to increase the creep strength of γ-TiAl alloys. However, besides embrittlement the thermal stability of the fine precipitates against coarsening, e.g., under long-term creep conditions, has to be proved.

### 2.1. Design Concept of TNM Alloys

In order to increase the economic feasibility of wrought processing for γ-TiAl components an alloy is needed which can be processed near conventionally, which means that conventional forging and rolling equipment with minor and inexpensive modifications can be used. Here, the major challenge is forging of small parts, e.g., turbine blade pre-forms, or rolling of thin sheets which, in comparison to large ingots, possess only a small amount of stored heat energy. In addition, a fine-grained and isotropic casting microstructure is favorable to both ingot breakdown and secondary forming operations. The alloys should be designed to allow robust industrial heat treatments, i.e., the material must tolerate a specified, and technologically realistic, variation of the constituting elements, without pronounced changes of phase transition temperatures and phase volume fractions as well as related variations in mechanical properties. In this context, the Al-content is of particular importance. The desired microstructures should be achieved by simple heat treatments which can be conducted at an industrial scale and which are almost independent from the geometrical dimension of the final part. Furthermore, the microstructure must show a resistance against microstructural changes during long-term exposure to service temperatures in the range of 600–750 °C. In addition, the machinability of the material by a wide variety of techniques (turning, mechanical and chemical milling, etc.) must be guaranteed. Finally, the alloy should show balanced mechanical properties (strength and ductility, fracture toughness, creep resistance) and acceptable oxidation resistance.

From these mentioned requirements, which represent the most important ones only, the following demands on the alloy are deduced: (a) after casting and solidification the alloy should possess a refined equiaxed microstructure showing no significant casting texture, see Figure 5. Examples of γ-TiAl based alloys which show a refined cast microstructure as well as their design concepts were reported by Zhang *et al.*,[99–101] Chladil *et al.*,[25] and Imayev *et al.*[63] along with other research groups, e.g., see ref;[5,12,102,103] (b) the composition of the alloy must be defined to ensure a solidification path according to $L \rightarrow L + \beta \rightarrow \beta \rightarrow \ldots$, instead of a peritectic solidification, i.e., $L \rightarrow L + \beta \rightarrow \alpha \rightarrow \ldots$, which is prone to segregation.[64] Additionally, alloys which solidify completely via the β-phase show a $\beta \rightarrow \alpha$ phase transformation, exhibiting the Burgers orientation relationship $(\bar{1}10)_\beta // (0002)_\alpha$ and $[111]_\beta // [11\bar{2}0]_\alpha$.[104,105] According to this, within a single β-grain α-grains with up to 12 orientation variants can be formed, leading to an intrinsic grain refinement which is not possible in case of a peritectic solidifying TiAl alloy; (c) during ingot breakdown, which might be obsolete in case of a homogeneous fine-grained and isotropic casting microstructure as well as secondary hot-forming operations, a significant volume fraction of disordered bcc β-phase should be present providing a sufficient number of independent slip systems. Thus, it may improve the deformability at elevated temperature, where, e.g., processes such as extrusion, forging, and rolling are carried out. In addition, the presence of a sufficient volume fraction of β-phase at hot-working temperature helps to suppress grain growth during soaking and multi-step forming operations. A number of authors[25,26,29,102,106–112] have demonstrated that by stabilizing the β-phase through alloying with Nb, Ta, Mo, V, or other elements, a significant improvement in hot-workability can be achieved. Takeyama and co-workers,[61,106,108] who were the first pointing out the use of β-phase for the development of wrought TiAl alloys, demonstrated that ingot breakdown of a β-phase containing TiAl is possible on a conventional forge with the associated high deformation rates. At service temperature, however, the volume fraction of the $\beta_o$-phase, which then shows an ordered B2 structure, should be insignificant in order not to deteriorate creep properties,[5,90] a design criteria which was often overlooked; (d) in order to avoid uncontrollable grain coarsening effects during the adjustment of the microstructure of both cast and forged material by subsequent heat treatments the existence of a single α-phase region at elevated temperatures should be avoided, thus transitions such as $\alpha + \gamma \rightarrow \alpha$, must be suppressed. Another possibility is to keep the α-phase region very small. In this case, the single α-phase field can be passed without significant grain coarsening as long as the dissolution kinetics of the β-phase is decelerated by the presence of alloying elements which show a low diffusibility, e.g., Mo and Nb. In addition, the slope of the γ-solvus (α-transus) line should be small. A small dependence of $T_{\gamma,\mathrm{solv}}$ on the Al concentration renders deviations in the Al content as well as variations in heat treatment temperatures uncritically. For example, a high Nb bearing TiAl alloy with the baseline composition of Ti–45Al–5Nb shows a steep slope of the α-transus line. For this alloy a variation in Al content in

  

ADVANCED ENGINEERING MATERIALS



the range of ±0.5 at% can be converted into a shift of the γ-solvus temperature of about 30 °C (from the highest to the lowest Al content). The negative effect of such a shift in $T_{\gamma,solv}$ on the forging behavior of Ti–45Al–5Nb is reported in ref.[29] Obviously, such alloys require stringent control of composition and processing parameters; (e) the alloys should provide a well-balanced phase ratio of γ-TiAl, $\alpha_2$-$Ti_3Al$, and $\beta_o$-TiAl which can be converted in designed microstructures (D, NL, FL) by means of simple and reproducible heat treatments; (f) finally, the appearance of decomposition products of the ordered $\beta_o$-phase, e.g., ω-phase,[113] has to be taken into account which might cause embrittlement.

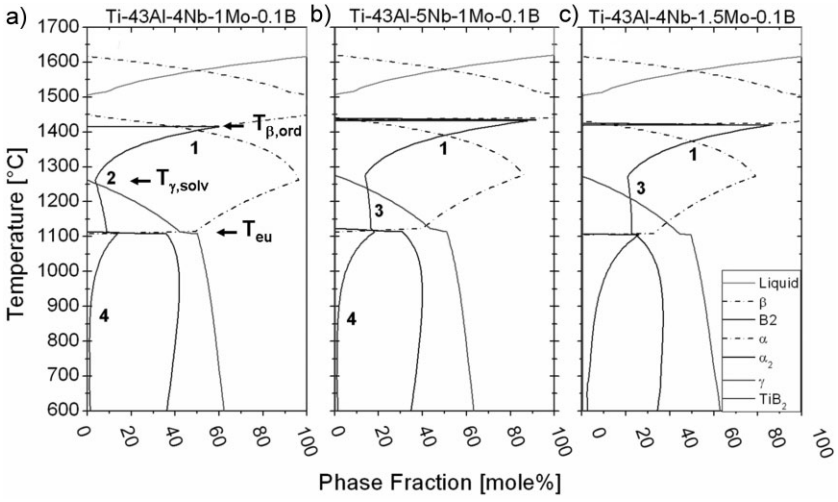


*Fig. 7. Calculated phase fractions as a function of temperature for three different β-stabilized Ti–43Al–Nb–Mo–0.1B alloys including 450 mass-ppm O.[26] For the calculation the database of Saunders[114] was used. Note the temperature dependence of the β/$\beta_o$-phase. In (a) the position of the eutectoid temperature ($T_{eu}$), the γ-solvus temperature ($T_{\gamma,solv}$) and the ordering temperature of the β-phase ($T_{\beta,ord}$) is indicated. All three alloys show an adjustable β/$\beta_o$-phase fraction above ≈1275 °C (''1''), but only alloy Ti–43Al–4Nb–1Mo–0.1B exhibits a pronounced minimum (''2'') of this phase above the eutectoid temperature (here at ≈1115 °C), whereas the other two alloys show almost unchanging values (''3''). Below $T_{eu}$ the β/$\beta_o$-phase fraction decreases with decreasing temperature and seems to vanish at about 600 °C in case of alloys Ti–43Al–4Nb–1Mo–0.1B and Ti–43Al–5Nb–1Mo–0.1B (''4''). $T_{eu}$: eutectoid temperature; $T_{\gamma,solv}$: γ-solvus temperature; $T_{\beta,ord}$: ordering temperature of the β-phase.*

In order to select an alloy which fulfils the demands as defined in (a) to (f), to the authors knowledge, for the first time a computer-aided method was applied for the design of an engineering γ-TiAl based alloy which eventually – after further optimization – became the so-called TNM™ alloy. To this end, thermodynamic calculations based on the CALPHAD method were conducted for the prediction of the constituent phases and the related phase transition temperatures.[25,26] The software package ThermoCalc® was applied using a commercial TiAl database developed by Saunders.[114] Details regarding modeling can be found in the reviews of Ansara[115] and Saunders and Miodownik.[116] Whereas the database is an excellent prediction tool for low alloyed 2nd generation alloys, it was found to poorly describe the transition temperatures and phase proportions in high Nb bearing γ-TiAl based alloys as reported in ref.[73,117] Furthermore, important elements such as C are not yet included in the database. Therefore, it should be pointed out that the calculations used for alloy design were conducted to study alloying trends rather than to obtain absolute values regarding phase fractions and transition temperatures. In the last years, however, the thermodynamic details of the Ti–Al–Nb system, relevant for the design of advanced TiAl alloys, have been investigated by Witusiewicz *et al*.[118,119] and Liu *et al*.[120] The thermodynamic functions for the phases of interest (γ, $\alpha/\alpha_2$, $\beta/\beta_o$) assessed in their studies can be used to calculate up to a Nb mole fraction of 0.1. The results of modeling have shown a good agreement with experimental observations.[120] Exemplarily, Figure 7 shows the calculated phase fractions as a function of temperature for three different β-stabilized γ-TiAl based alloys. The three alloys have a constant Al concentration (43 at%), but different contents of β-stabilizing alloying elements (Nb, Mo). The concentration of B is kept constant with 0.1 at%. Before Figure 7 will be discussed in detail, the role and the main effects of the selected alloying elements are addressed. Like Nb, which is outlined above, Mo is a β-stabilizing element in the Ti–Al system, which raises the activation energy of diffusion in both γ-TiAl and $\alpha_2$-$Ti_3Al$, but exhibits a much higher partition coefficient $k_{\beta\alpha}$ than Nb.[61] It must be taken into account that phases, when stabilized by such slow-diffusing elements, are expected to exhibit sluggish dissolution behavior. The B content of 0.1 at% was selected to ensure a grain refining effect during solidification[121–123] as presented in Section 4 (Figure 16c). Boron, which tends to form very stable borides, is also beneficial in case of heat treatments conducted at high temperatures. Here, the borides retard grain coarsening by pinning the grain boundaries. In addition, the borides favor the formation of the lamellar microstructure ($\alpha \rightarrow \alpha + \gamma$) over the massive transformation ($\alpha \rightarrow \gamma_M$) by heterogeneous nucleation of γ-TiAl lamellae.[121,122]

Figure 7a–c demonstrate that all chosen alloys solidify entirely via the β-phase. Figure 7 predicts for TNM alloys an ordering reaction $\beta \rightarrow \beta_o$ at about 1410–1420 °C ($T_{\beta,ord}$), depending on the actual alloy composition, which contradicts the excellent hot-working behavior observed at significantly lower temperatures.[26] In order to determine the ordering temperature of the β-phase, in situ neutron diffraction measurements were conducted in the temperature range from 900 to 1450 °C. It was found that in a Ti–43Al–4Nb–1Mo–0.1B alloy ordering of the β-phase occurs around 1210 °C.[37] From comparison of the phase fractions of the three different compositions shown in Figure 7 and additional experimental investigations it was found that Mo is a 4 times stronger β-stabilizer than Nb, which agrees with the results of other studies.[5,63,124–126] Thus, the β-equivalent in TNM alloys can be quoted as $\beta_{eq} = Nb + 3.9$ Mo (in at%). Furthermore, for all three alloys the thermodynamic calcula-

  

tion shows a minimum of the mole fraction of the β-phase at around 1275 °C. Above this temperature the fraction of β-phase strongly increases with temperature (see ''1'' in Figure 7). However, at the temperature where the minimum of β-phase appears, Ti–43Al–4Nb–1Mo–0.1B shows the smallest fraction of β-phase and only this alloy variant exhibits a pronounced ''C-shaped'' course of the β-phase (see ''2'' in Figure 7a). By increasing the amount of Nb or Mo by 1 or 0.5 at%, respectively, the mole fraction of the β-phase in its minimum at 1275 °C is considerably increased (see ''3'' in Figure 7b and c). Below the temperature of its minimum the mole fraction of the β-phase slightly increases (Figure 7a) or shows an approximately unchanging value (Figure 7b and c). It should be emphasized that the magnitude of the volume fraction of the β-phase at the minimum is of particular interest as far as heat treatments subsequent to the forging process are concerned (see Section 4.1). Below the eutectoid temperature ($T_{eu} \approx 1115$ °C) the ordered $\beta_o$-phase fraction decreases with decreasing temperature and seems to vanish at about 600 °C in case of alloys Ti–43Al–4Nb–1Mo–0.1B and Ti–43Al–5Nb–1Mo–0.1B, see ''4'' in Figure 7a and b, respectively. It should be noted that all three alloys exhibit an adjustable volume fraction of the β-phase in the temperature range where hot-working of γ-TiAl based alloys is usually performed. However, only alloy Ti–43Al–4Nb–1Mo–0.1B shows the potential that the appearing β-phase can almost be removed by a subsequent heat treatment (see Section 4.1). To this end, the annealing temperature must correspond to that temperature where the minimum of the β-phase occurs, i.e., to temperature ''2'' in Figure 7a. At such a high temperature the dissolution kinetic of the β-phase is rather fast, thus allowing short annealing times.[28] In principle, removal of the β-phase below the eutectoid temperature is possible, but would require long, and thus costly, annealing times due to the sluggish dissolution behavior of the Mo and Nb containing β-phase. From the phase predictions displayed in Figure 7 it is obvious that none of the three alloys exhibit a single phase region at temperatures below 1400 °C. From additional thermodynamic calculations and experimental verification a TNM alloy with a nominal composition of Ti-43.5Al-4Nb-1Mo-0.1B shows the best match with the demands defined at the beginning of this chapter. It must be kept in mind that Figure 7 predicts phase conditions present under thermodynamic equilibrium. However, engineering γ-TiAl based alloys, when processed under technical relevant conditions, always show a more or less distinct deviation from phase equilibrium.

In Figure 8a and b, the comparison of a calculated phase fraction diagram to an experimentally determined one is given. The investigated TNM alloy was produced by means of powder metallurgy[127] and the actual composition is Ti–43.9Al–4.0Nb–0.95Mo–0.1B. For the experimental investigation of the course of the phase fractions as a function of temperature, heat treatments following quantitative metallography as well as in situ diffraction measurements were conducted employing synchrotron radiation.[27,30] Whereas

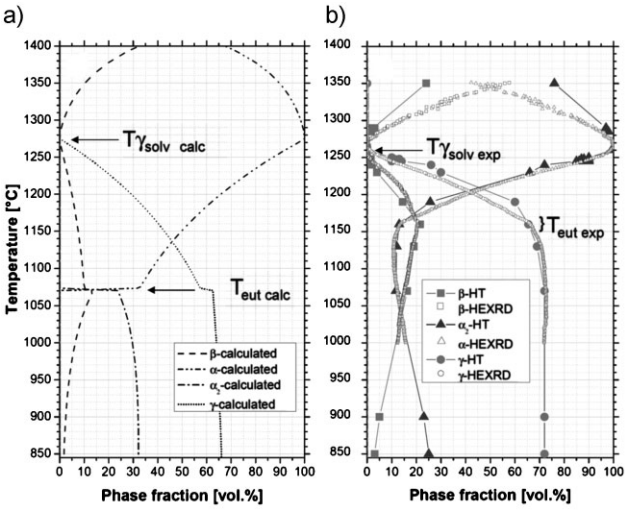


*Fig. 8. (a) Calculated phase fractions as a function of temperature for a TNM alloy with a composition of Ti–43.9Al–4.0Nb–0.95Mo–0.1B; (b) the results of in situ diffraction measurements using synchrotron radiation (open symbols) and quantitative analysis of heat-treated specimens (solid symbols).[27]*

the γ-solvus temperature agrees well with experimental data derived from quantitative analysis of heat-treated specimens and in situ HEXRD diffraction experiments, the eutectoid temperature is significantly underestimated by the thermodynamic calculation. The course of the experimental phase fractions around $T_{\gamma,solv}$ is in agreement with the calculated data, but differ increasingly with increasing distance to the γ-solvus temperature. For more detailed information concerning this study and powder metallurgical processed TNM the reader is referred to ref.[27,128] It should be pointed out that annealing experiments to determine phase volume fractions are rather time consuming and large numbers of samples are required, whereas in situ HEXRD investigations can be conducted and evaluated considerably faster.[30,36] In the framework of several research projects a large number of differently composed cast TNM alloys were analyzed as the example shown in Figure 8b. The allocated data were then used to create a three-dimensional phase diagram as displayed in Figure 9 which has been proven useful to evaluate deviations in alloy composition on transition temperatures and to define the parameters for both hot-working and heat treatments as well as to establish a thermodynamic database for TNM alloys which possesses a high predictive accuracy.[129,130]

## 3. Processing of γ-TiAl Based Alloys

The processing routes on industrial scale established for wrought γ-TiAl based alloys are summarized in Figure 10 along with examples taken from ref.[1,2,4,8,9,17] These references, supplemented by ref.,[10,12,26,28,42,131,132] provide an insight into the technology established for this class of materials. In the last two decades a variety of different 2nd and 3rd generation γ-TiAl based alloys were processed according to the routes displayed in Figure 10, where the focus was put on ingot metallurgy (IM)

  

ADVANCED ENGINEERING MATERIALS



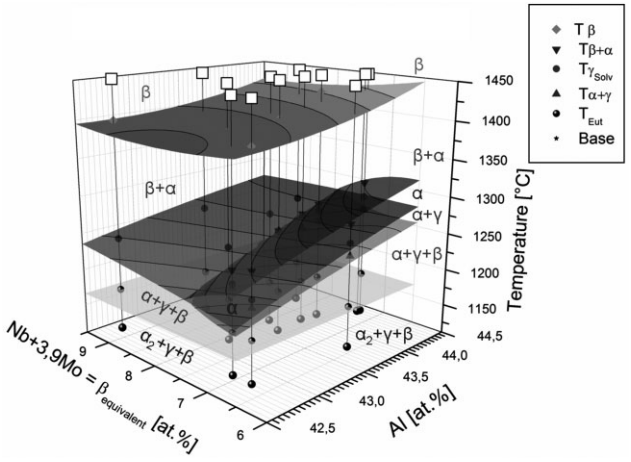


*Fig. 9. Three-dimensional phase diagram for the TNM alloy family. The abscissas show the Al concentration and the β-equivalent ($\beta_{eq} = Nb + 3.9Mo$).[129]*

and forging. In general, hot-working of TiAl alloys is conducted exclusively above their brittle-to-ductile transition temperature, i.e., at temperatures considerably higher than 700 °C and can be divided in primary and secondary hot-working steps. The aim of primary hot-working of cast ingots is to convert (or breakdown) the coarse-grained microstructure into a fine-grained and uniform microstructure suitable for subsequent wrought processing or heat treatments. This is accomplished by employing hot-working parameters at which dynamic recrystallization is prevalent and macroscopic as well as microscopic damage can be neglected, i.e., at temperatures between $T_{eu}$ and $T_{\alpha}$ and at relatively low deformation rates. In order to simulate the microstructure development during hot-working, e.g., forging, a finite element cell model was generated as reported in ref.[50,133] The evolution of texture during rolling, extrusion, forging, and subsequent heat treatments was investigated for different TiAl alloys, e.g., see ref.[65–68,134] and references therein. During the last decade several wrought γ-TiAl alloys with complex alloy compositions have been developed.[7–9,11,87] These alloys exhibit excellent mechanical properties, but show narrow processing windows. Therefore, these alloys can be forged only under isothermal conditions.[19,29] However, isothermal forging of γ-TiAl based alloys must be performed at high temperatures, requiring special dies and environmental conditions which increase manufacturing costs. Therefore, TNM alloys have been developed which are equally suited for hot-die forging under near conventional conditions[26,28] and isothermal forging.[135] In addition, the homogeneous and fine-grained microstructure obtained after solidification offers the opportunity to omit the cost-intensive ingot breakdown. Figure 11a shows a turbine blade after the last forging step using a hot-die forging process. The forging process is conducted at standard atmosphere.[136] Figure 11b exhibits a part made of TNM alloy which was hot-forged using a one-shot process.[137] The processing routes acquired for TNM alloys on an industrial scale, except sheet rolling which was conducted on a laboratory roller mill, are indicted in Figure 10 by bold lines.

TiAl alloy ingots can be produced either by vacuum arc remelting (VAR)[2,138] or plasma arc melting (PAM).[139] Recently, GfE – Metalle und Materialien GmbH (Germany) has introduced a production technique for 2nd and 3rd generation TiAl alloys, which combines VAR skull melting with centrifugal casting in permanent moulds,[140] as schematically shown in Figure 12a. The advantage of this process is the possibility to produce adjusted feed stock materials for both hot-working and investment casting directly from the ingot with a remarkably improved materials yield. The slugs, as displayed in Figure 12b, exhibit a satisfying microstructural homogeneity, homogeneous alloying element distribution as well as concentrations of unwanted impurities (O, N) well below 700 wt-ppm. In conclusion, it can be stated that a significant world-wide progress in γ-TiAl ingot processing on industrial scale has been achieved over the last decade. Processing and quality control have reached a level comparable to that of commercially used aerospace materials. However, a particular challenge for the years to come is to develop effective strategies for cost reduction which certainly will demand the implementation of recycling concepts for γ-TiAl based alloys.[141]

Due to lack of space this review cannot enlarge on recent developments in the technology of TiAl alloys, e.g., selective laser melting, joining, and oxidation protective coatings. Here the reader is referred to a large number of publications which can be easily accessed, e.g., by means of Scopus.

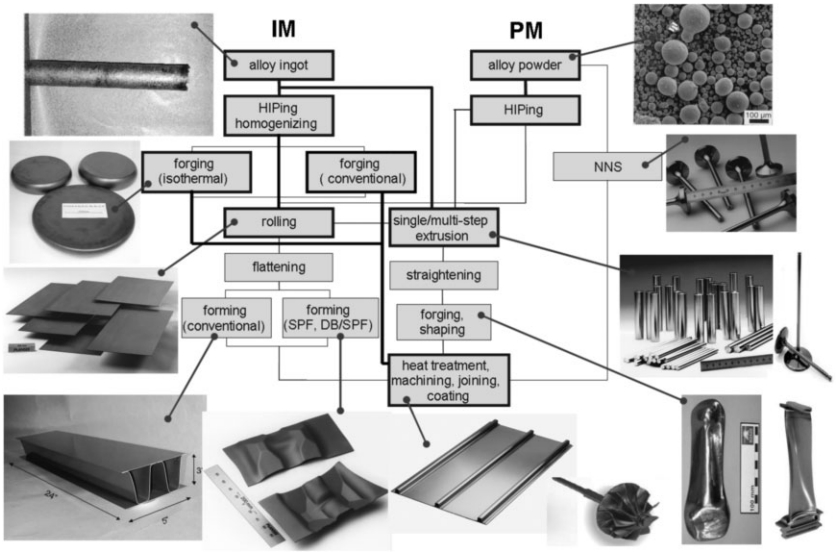


*Fig. 10. Manufacturing and processing routes established for wrought γ-TiAl based alloys on an industrial scale as well as examples of finished and semi-finished products. The bold lines highlight the routes developed for TNM alloys so far. Corresponding microstructures are shown in Figure 16. IM, ingot metallurgy; PM, powder metallurgy; HIP, hot-isostatic pressing; DB, diffusion bonding; SPF, superplastic forming; NNS, near-net shape.*

  

REVIEW

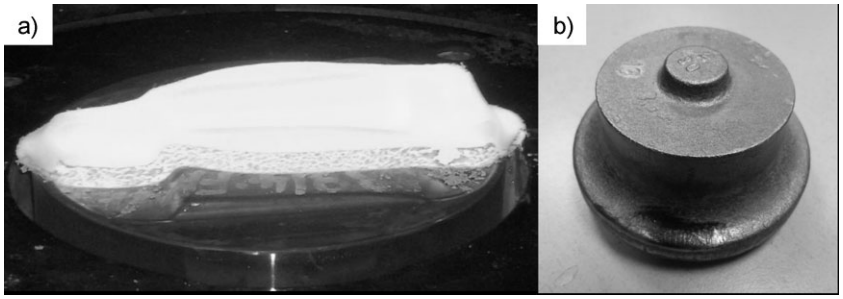


*Fig. 11. (a) Turbine blade after the final forging step employing a hot-die forging process. The forging process is conducted at standard atmosphere;[1136] (b) TNM forging which was made in a single-shot process.[1137]*

## 4. Adjustment of Micro- and Nanostructures by Thermo-Mechanical Processing and Heat Treatments

In this chapter, general information on microstructural evolution in intermetallic titanium aluminides are highlighted, whereas Section 4.1 focuses on the behavior of TNM alloys exclusively. Four different important types of microstructures, obtained in engineering γ-TiAl based alloys, are shown in Figure 13. The depicted examples were adjusted in a 2nd generation alloy by means of heat treatments conducted on a fine-grained starting material.[2,23] Generally, the influence of microstructure on mechanical properties of γ-TiAl based alloys can be summarized as follows: coarse-grained FL and NL microstructures exhibit relatively high fracture toughness and creep resistance, but poor tensile ductility especially at room temperature.[2,42,47] Comparably fine-grained equiaxed NG and D microstructures with only small amounts of lamellar colonies show low fracture toughness and creep resistance but moderate tensile ductility at ambient temperatures. A description of the different intrinsic and extrinsic mechanisms which contribute to the fatigue crack growth resistance in TiAl alloys is given in ref.[1,12,42,47,142–144] This inverse correlation between tensile properties and resistance to fracture (fracture toughness) requires a careful selection of the microstructure which makes microstructural optimization important for achieving balanced engineering properties. For engineering γ-TiAl based alloys with compositions given in Equation (2), e.g., TNM alloys, the optimum balance between fracture toughness and creep resistance on one side and room temperature tensile ductility on the other side is expected for microstructures composed of relatively small lamellar colonies (50–100 μm in diameter) exhibiting narrow lamellar spacing and a small volume fraction of globular γ-TiAl and $\beta_o$-TiAl grains[28] (see Section 4.1). In order to realize these so-called designed NL microstructures by using industrial annealing furnaces, the transformation behavior of γ-TiAl alloys must be known exactly, e.g., the variation of the γ-solvus temperature within the limits of the specified composition range.

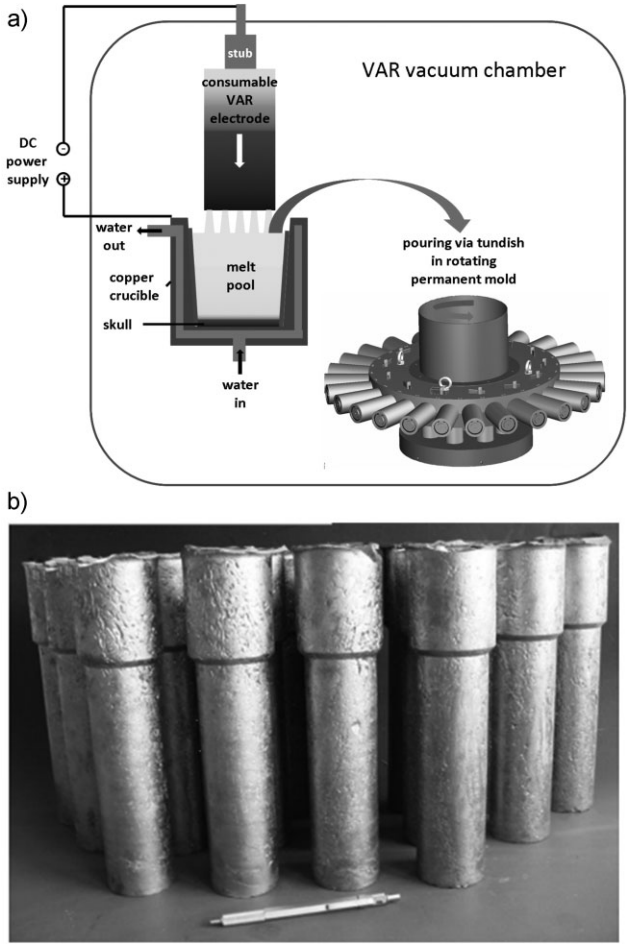


*Fig. 12. (a) Schematic illustration of the VAR skull melting process employed by GfE Metalle und Materialien GmbH (Germany) for the production of TNM alloys.[1140] Subsequently, the melt is processed by means of centrifugal casting in permanent moulds; (b) TNM slugs after removing from the moulds. A representative microstructure of a Ti–43.5Al–4Nb–1Mo–0.1B alloy is shown in Figure 16a.*

Annealing of a fine-grained starting material above the eutectoid temperature leads to the formation of a NG microstructure (Figure 13). This microstructure consists of equiaxed γ-TiAl grains and – in accordance to the lever rule – a small amount of $\alpha_2$-$Ti_3Al$ situated at triple points and grain boundaries. Heat treatments in the middle of the $(\alpha+\gamma)$ region result upon cooling to room temperature in the evolution of a D microstructure composed of globular γ-TiAl grains and $\gamma/\alpha_2$-colonies, but also a small volume fraction of $\alpha_2$-$Ti_3Al$ precipitates at the boundaries of the colonies and γ-grains. The γ- and $\alpha_2$-lamellae within the colonies possess the following crystallographic relationship: $(111)\gamma//(0001)\alpha_2$ and $\langle 110]\gamma//\langle 11\bar{2}0\rangle\alpha_2$.[145] This so-called Blackburn relationship becomes quite clear, when the atomic matching of the $(111)\gamma$- plane and the $(0001)\alpha_2$-basal plane is taken into account. With increasing annealing temperature in the $(\alpha+\gamma)$ phase field region the proportion of lamellar colonies increases. The lamellar spacing in the colonies depends strongly on the applied cooling rate.[23,146] NL or FL microstructures are formed upon cooling when wrought

  

ADVANCED ENGINEERING MATERIALS



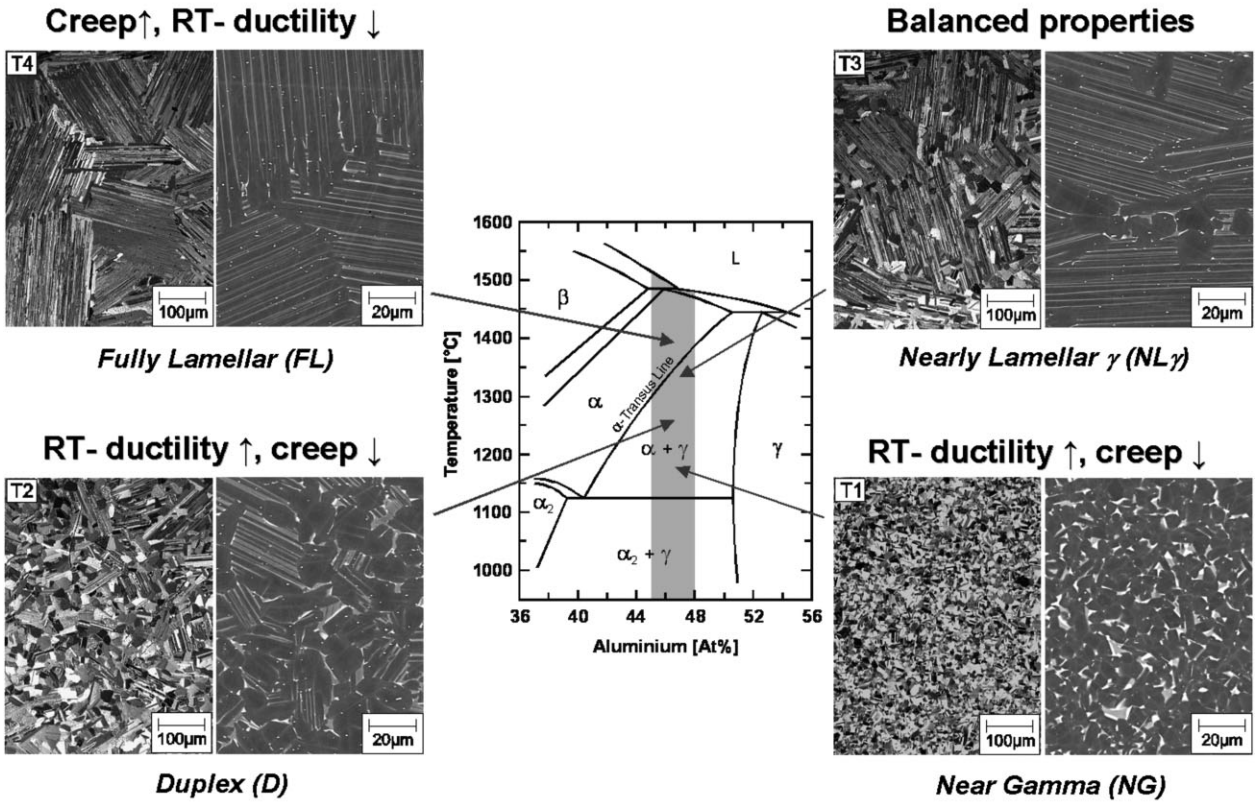


*Fig. 13. Mid-section of the binary Ti–Al phase diagram and representative microstructures obtained by means of heat treatments within the α and (α + γ) phase field.[23] Note that the left half of the microstructural image represents a light-optical microscope (LOM) image, whereas the right half is a SEM image taken in BSE mode, i.e., γ-TiAl appears dark, whereas $\alpha_2$-$Ti_3Al$ shows a light contrast. Heat treatments: little above the eutectoid temperature ($T_{eu}$) → near gamma (NG) microstructure; between $T_{eu}$ and α-transus temperature $T_\alpha$ → duplex (D) microstructure. The volume fraction of lamellar grains depends on the heat treatment temperature relative to $T_{eu}$ and $T_\alpha$; just below $T_\alpha$ → nearly lamellar (NL) microstructure. The designation NLγ stands for a NL microstructure exhibiting a defined volume fraction of globular γ-grains; above $T_\alpha$ → FL microstructure. The impact of the various microstructures on RT ductility and creep resistance is indicated (see text).*

γ-TiAl based alloys are heat treated about 10 °C below or 10–20 °C above $T_\alpha$, respectively. Here, it should be noted that heat treating in the single α-phase field region can bear the danger of uncontrolled grain growth due to the absence of a second phase. Especially for plain γ-TiAl based alloys, colony sizes in the range of 100–500 µm are readily obtained after annealing above $T_\alpha$ for a few minutes only. However, such coarse-grained FL microstructures cannot be used because of their inherently low tensile ductility at room temperature. In this context, B proved to be very beneficial for obviating uncontrolled growth of α-grains when cast as well as wrought γ-based alloys are heat-treated above $T_\alpha$.[2,42,47] The transformation of the high-temperature α-phase to lamellar α + γ phases upon cooling is well known. The reaction occurs in the (α + γ) phase field by introduction of stacking faults in the hexagonal α-phase (spreading of Shockley partial dislocations on the basal planes) which produce the correct stacking sequence for the $L1_0$ structure, followed by diffusional growth and chemical equilibration of the γ-phase.[145,147] It has been shown that lamellar formation occurs rapidly below $T_\alpha$, however, the degree of undercooling required for nucleation of the reaction is strongly dependent upon cooling rate, alloy composition, and α-grain size.[148] From such studies, continuous cooling transformation (CCT) diagrams have been established for several γ-TiAl based alloys as reported in ref.[146,148] For example, Figure 14 schematically shows the CCT diagram of a Ti–46Al–9Nb alloy.[149] At slow cooling, e.g., furnace cooling (FC), from the single α-phase field region a FL microstructure is formed by diffusion-assisted processes as noted above. Increasing the cooling rate, e.g., air cooling (AC), leads to a decrease of the average lamellar spacing in the $\gamma/\alpha_2$-colonies and to the onset of massive transformation. The microstructure then consists of lamellar colonies with a fraction of massive $\gamma_m$-TiAl grains situated at colony boundaries. In a massive transformation, the disordered hexagonal α-phase transforms massively into the $\gamma_m$-phase which exhibits a high density of internal boundaries and defects.[150] Since the $\alpha \rightarrow \gamma_m$ transition occurs without any change in composition,[151] the product $\gamma_m$-phase must be depleted in Al. At a certain critical cooling rate, e.g., oil quenching (OC), the α-phase is completely transformed to $\gamma_m$ (Figure 14). XRD studies on fully massively transformed Ti–49Al–9Nb samples have shown that the $\gamma_m$-lattice is almost face-centered cubic.[152] This might be a consequence of high internal stresses and due to partially wrong site occupation of the constituting atoms in the $\gamma_m$ lattice. Indeed, ab initio calculations have shown that Ti and Nb atoms on Al-sites reduce the $c/a$-ratio of the tetragonal TiAl cell to ≈1.[153] From

  

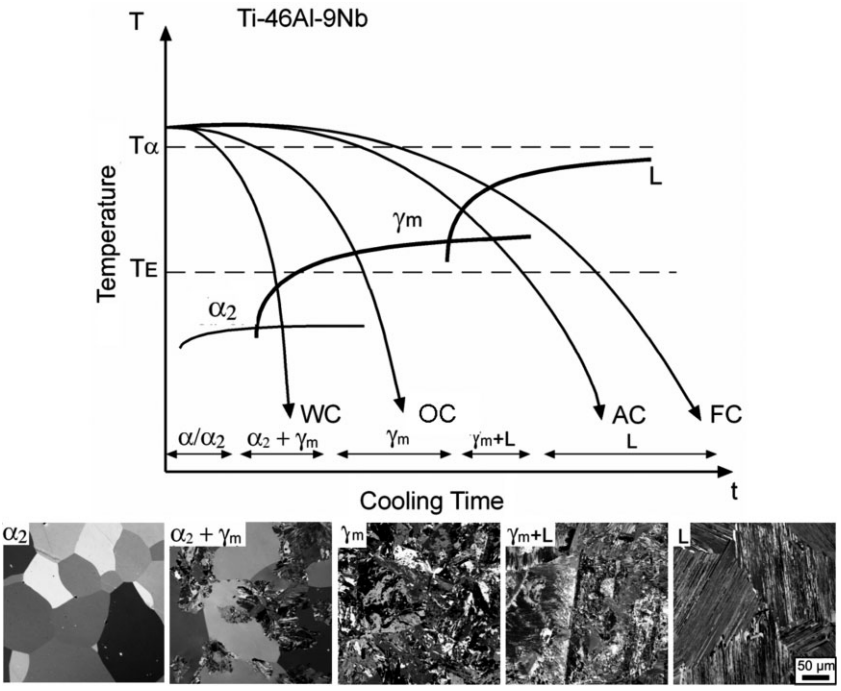


*Fig. 14. Schematic CCT diagram of a high Nb bearing γ-TiAl based alloy, showing the microstructures which have formed as a result of different cooling rates.[149] FC, furnace cooling; AC, air cooling; OC, oil cooling; WC, water cooling.*

a technological point of view, a massive phase transformation combined with a subsequent heat treatment can be used for the refinement of coarse-grained microstructures and to promote the formation of special types of lamellar microstructures as reported in ref.[152,154] At very high cooling rates, e.g., by quenching in water (WC), the massive transformation in Ti–46Al–9Nb can be entirely suppressed (Figure 14). At room temperature the microstructure then consists of supersaturated $\alpha_2$-$Ti_3Al$ grains, because the $\alpha \rightarrow \alpha_2$ ordering reaction cannot be prevented even at very high cooling rates.[34] Such a material condition can be used to adjust nanometer-scaled $(\alpha_2 + \gamma)$ lamellar microstructures by decomposition of the supersaturated $\alpha_2$-phase during a subsequent ageing treatment below $T_{eu}$.[83,155] For example, for TNM alloys two-step heat treatments have been developed which exploit ageing of supersaturated $\alpha_2$-$Ti_3Al$ grains to adjust high creep strength (see Section 4.1).[28] Exemplarily, Figure 15a shows a TEM image of a Ti–45Al–7.5Nb specimen which first was oil quenched from the single α-phase field region. In a second step, the sample was continuously heated to 790 °C at a rate of 20 °C $min^{-1}$, immediately followed by oil cooling. The TEM image, taken in dark field condition, shows ultrafine γ-lamellae which possess a Blackburn-relationship with the $\alpha_2$-$Ti_3Al$ matrix.[54] As a detail, Figure 15b depicts a high-resolution (HR) TEM image of a γ-TiAl lath which terminates within a $\alpha_2$-$Ti_3Al$ grain. It should be noted, however, that most of the γ-TiAl laths are terminating at grain/colony boundaries. The beam direction is $[\bar{1}10]\gamma // [\bar{1}\,\bar{2}\,\bar{1}0]\alpha_2$ and, therefore, the $(111)\gamma // (0001)\alpha_2$ interfaces, indicated by solid lines, are edge on. Some steps exist along this interface with a height corresponding to a $(111)\gamma$ lattice plane distance. At the terminating end of the γ-TiAl lath, the lattice mismatch between the γ-TiAl and the $\alpha_2$-$Ti_3Al$ phase can be compensated by transformation dislocations that have the Burgers vector of a Shockley partial dislocation and occur on every other close packed plane. Modeling of the formation of γ-TiAl lamellae from supersaturated $\alpha_2$-$Ti_3Al$ grains has been performed by Fischer *et al.* [54] Their theoretical concept allows the prediction of both the onset of formation of a γ-TiAl lamella as well as its thickness.

Besides the transformation products shown in Figure 14 various other microstructural features have been reported for

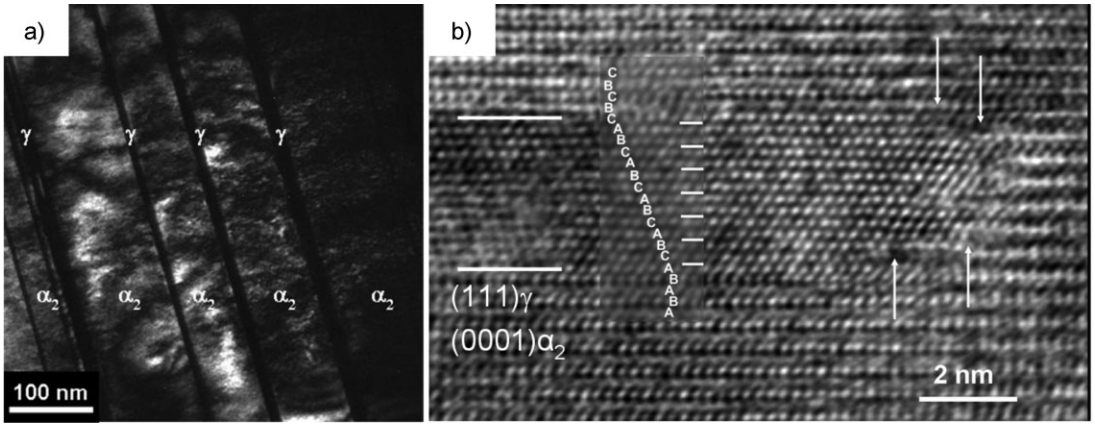


*Fig. 15. (a) TEM dark field image of a fine lamellar structure in a Ti–45Al–7.5Nb specimen using the $(0001)\alpha_2$ diffracted beam (see text). The positions of both γ-TiAl and $\alpha_2$-$Ti_3Al$ laths are indicated. The microstructure was adjusted by ageing a strongly supersaturated $\alpha_2$-$Ti_3Al$ matrix; (b) HRTEM image of a γ-lamella that terminates within the supersaturated $\alpha_2$-$Ti_3Al$ matrix. The stacking sequence of the close packed planes is indicated. The $(111)\gamma//(0001)\alpha_2$ habit planes are marked by full lines. The arrows point to misfit dislocations. Beam direction $= [\bar{1}10]\gamma//[\bar{1}\,\bar{2}\,\bar{1}0]\alpha_2$.[54]*

  

ADVANCED ENGINEERING MATERIALS



γ-TiAl based alloys, such as Widmannstätten,[148,156–158] feathery,[148] and martensitic microstructures[12,108] as well as the appearance of transition and other complex phases which occur during phase transformations and annealing treatments, respectively.[12,159–164]

### 4.1. Micro- and Nanostructure and Mechanical Properties of TNM Alloys

As described in Section 2 it has been demonstrated that, by stabilizing the β-phase through alloying with Nb, Ta, Mo, or other elements, an improvement in hot-workability can be achieved, but also novel types of microstructures can be adjusted by exploiting a multitude of solid-state transformations. In the following, the evolution of the micro- and nanostructure in TNM alloys and their characterization will be reviewed. At the end of this paragraph some examples will be given how the mechanical properties relate to the adjusted microstructures.

Figure 16a shows a SEM image of the microstructure of the TNM alloy Ti–43.5Al–4Nb–1Mo–0.1B in the as-cast condition. Note that all specimens used for the compilation of Figure 16 were prepared metallographically according to ref.[128] The material shown in Figure 16a was produced by means of VAR skull melting and centrifugal casting in permanent moulds (see Section 3 and Figure 12). The microstructure can be explained by a complete solidification via the β-phase as predicted in Figure 7. It consists of lamellar $(\gamma + \alpha_2)$-colonies with a colony diameter well below 100 μm. Because of the high cooling rate the lamellar spacing is small and cannot be resolved at the used magnification. The ordered $\beta_o$-phase is mainly located along colony boundaries and only a small volume fraction is present within the colonies. In addition, the existence of rod-shaped (Ti, Nb, Mo)-monoborides was detected. EDX analysis has provided evidence that the $\beta_o$-phase is more enriched in Mo than in Nb, which confirms that Mo exhibits a higher partition coefficient $k_{\beta\alpha}$ than Nb. From the appearance of the microstructure and the phases present the following solidification pathway is proposed $L \rightarrow L + \beta \rightarrow \beta \rightarrow \beta + \alpha \rightarrow \alpha + \gamma + \beta \rightarrow \alpha + \alpha_2 + \gamma + \beta_o \rightarrow \alpha_2 + \gamma + \beta_o$.[25,26] In as-cast condition the material shows a certain residual casting porosity and the phases occurring are far from thermodynamic equilibrium, both in composition and volume fraction.

In order to close casting porosity and to improve chemical homogeneity by diffusion processes, the material is subjected to hot isostatic pressing (HIPing) which is conducted at 1200 °C for 4 h at 200 MPa followed by furnace cooling. Figure 16b shows a representative as-HIPed microstructure. From comparison with Figure 16a it is evident that during HIPing a significant change in the microstructure has taken place. The present phase fractions correspond approximately to that predicted in Figure 7 for alloy Ti–43Al–4Nb–1Mo–0.1B. A large fraction of globular γ-TiAl grains is prevailing at the boundaries of the lamellar $\gamma/\alpha_2$-colonies, obviously the result of a phase transformation $\beta_o \rightarrow \gamma$. The increase of γ-TiAl phase in combination with diffusion processes has also led to noticeable coarsening of the lamellae within the colonies. Additionally, some $\alpha_2$-laths show fine precipitates of $\beta_o$-phase. Such precipitation reactions were also observed in other γ-TiAl based alloys which contain an effectual amount of β stabilizing elements.[108,162] HRTEM investigations have shown that the $\beta_o$-phase forms semi-coherent interfaces with the γ- and $\alpha_2$-phases and the following crystallographic relationship was determined: $(0001)\alpha_2 \,||\, (10\bar{1})\beta_o \,||\, (111)\gamma$ and $[1\bar{1}20]\alpha_2 \,||\, [111]\beta_o \,||\, [10\bar{1}]\gamma$.[165] In recent studies, it was demonstrated that the relatively fine-grained cast and HIPed microstructure can further be refined by subsequent heat treatments. Static annealing in the temperature range of 1250–1400 °C followed by AC[25,26] as well as cyclic heat treatments which are based on repetitive phase transitions[166] lead to colony sizes well below 50 μm.

The beneficial role of B in cast TNM alloys can be seen when Figure 16b is compared with Figure 16c. Figure 16c exhibits the microstructure of an alloy which was produced without adding the grain refining agent B.[98] Evidently, after casting and HIPing a coarse and inhomogeneous microstructure is present. Regarding the grain refining mechanisms which take place during solidification of B-containing TiAl alloys as well as the formation and type of the involved borides the reader is referred to ref.[123]

Figure 16d shows the microstructure of a HIPed Ti–49.9Al–4.0Nb–0.95Mo–0.1B powder consisting of globular γ, $\alpha_2$, and $\beta_o$ grains.[27] The microstructure impresses through structural homogeneity when, e.g., compared to that of cast and HIPed material (Figure 16b). The TNM powder was produced by Ar gas atomization using the electrode induction melting gas atomization (EIGA) technique.[127] In this technique, the pre-alloyed rod dips into a conical induction coil. Upon operation of the coil the tip of the road is heated and melts. In the center of a gas nozzle, the melt is then atomized by Ar gas. For compaction the powder with a particle size smaller than 180 μm in diameter was filled into cylindrical Ti cans. Subsequently, the capsules were evacuated, sealed and HIPed at 1250 °C for 2 h at 200 MPa, followed by furnace cooling. For information on powder metallurgy of TiAl in general and TNM alloys in particular the reader is referred to ref.[127,167] and ref.,[27] respectively.

In order to increase the high-temperature capability of TNM alloys the effect of C and other potential strengthening elements on tensile and creep strength was investigated. Because of the fact that C, which acts as α-stabilizer, is not included in the thermodynamic database, no trusted prediction of the solidification pathway and the course of the phase fractions as a function of temperature can be made as shown for other alloys in Figure 7. Figure 16e depicts the microstructure of a TNM alloy which is alloyed with 0.5 at% C. Although the C addition is rather small, the solidification character and, as a consequence, the appearing microstructure have changed dramatically. Due to the strong α-stabilizing character of C a considerable shift of the phase field regions in the TiAl–Nb–Mo alloy system has taken place, altering the

  

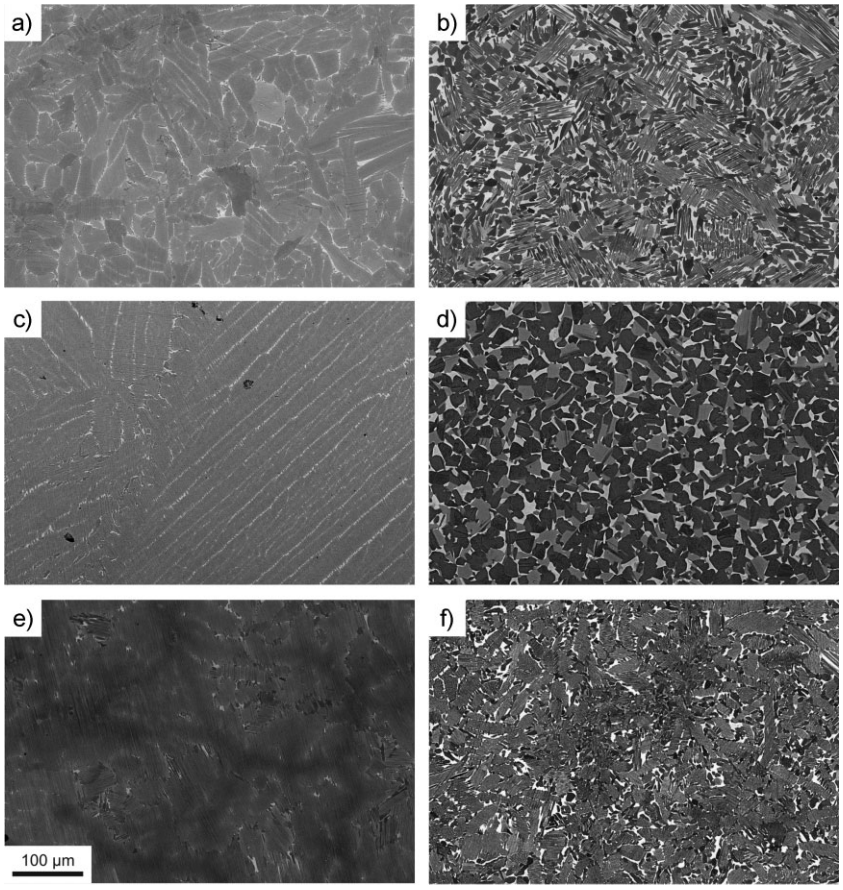


*Fig. 16. Microstructure of TNM alloys with differ in production process and chemical composition. (a) Ti–43.5Al–4Nb–1Mo–0.1B in as-cast condition; (b) cast material after HIPing for 4 h at 1200 °C and 200 MPa, followed by slow cooling; (c) cast and HIPed TNM alloy without B; (d) HIPed Ti–43.9Al–4Nb–0.95Mo–0.1B gas-atomized powder; (e) TNM alloy with 0.5 at% C, showing peritectic solidification when compared to (a); (f) TNM alloy with 0.5 at% C, where the α-stabilizing effect of C is compensated by a higher Mo content, retaining β-solidification. SEM image taken in BSE mode, i.e., γ-TiAl appears gray to dark, $\alpha_2$-$Ti_3Al$ light gray, and $\beta_o$-TiAl exhibits the brightest contrast. The metallographic specimens were prepared according to ref.[128]*

solidification path from β-solidification to a peritectic one.[98] In order to re-establish solidification via the β-phase, which leads to a fine-grained and chemically more homogeneous microstructure, the fraction of C must either be reduced to an appropriate level or compensated by adding a higher amount of β-stabilizing elements (Nb or Mo). As an example, Figure 16f shows the as-cast microstructure of a TNM alloy where the effect of C has been counterbalanced by an increase in Mo concentration. Evidently, the β-solidifying character was restored, leading to a fine-grained cast microstructure which is a distinguishing mark of TNM alloys (compare Figure 16f to Figure 16a).

In previous studies, it was shown that TNM alloys are equally suited for isothermal forging[135] as well as hot-die forging under near conventional conditions.[26] Recently, the technical feasibility of manufacturing a turbine blade by means of a near conventional hot-die process has been demonstrated. Detailed information regarding conventional hot-die forging is given in ref.[28,29] The good hot-workability is attributed to the high volume fraction of disordered bcc β-phase present during deformation in both the $(\alpha/\alpha_2+\beta/\beta_o+\gamma)$ and $(\alpha+\beta)$ phase field regions (see Figure 7 and 8). It is expected that during hot-working in these phase field regions the β-phase, even when in its ordered state, possesses a low flow stress and carries most of the deformation. Exemplarily, Figure 17 shows the flow curves of a cast and HIPed TNM alloy measured at 1200 and 1300 °C at a deformation rate of $5\times10^{-3}\,s^{-1}$.[168] The specimen deformed in the $(\alpha+\beta+\gamma)$ phase field region at 1200 °C reveals the effect of dynamic recrystallization in that the flow curve shows a flow stress maximum at a low strain (≈5%), followed by softening to an apparently constant stress level for a true strain higher than 60%. On the contrary, deformation within the $(\alpha+\beta)$ phase field at 1300 °C leads to a constant flow stress level immediately after the onset of compression. Such behavior reflects the dominance of dynamic recovery during deformation, which might be controlled by the high volume fraction of disordered β-phase present at this particular temperature. More information on the hot-working behavior, as investigated by an in situ diffraction method, is given below. The effects of strain rate $(\dot{\varepsilon})$ and temperature $(T)$ during high temperature deformation are often incorporated into the so-called Zener-Hollomon parameter $Z$, which is defined as ref.[169]:

$$Z = \dot{\varepsilon} e^{Q/RT} \tag{3}$$

where $Q$ is the apparent activation energy and $R$ the universal gas constant. For a TNM alloy with a nominal composition of Ti–43Al–4Nb–1Mo–0.1B an activation energy of 584 kJ mol$^{-1}$ was determined for the temperature range of 1000–1200 °C and strain rates ranging from 0.001 to 1 s$^{-1}$.[170] However, the authors gave no explanation for the occurrence of such high activation energy. Depending on the test conditions used, the parameter $Z$ can be related to the flow stress as reported in ref.[131,170–174] Regarding the deformation characteristics, microstructural evolution and kinetic aspects as well as the occurring deformation mechanisms in γ-TiAl based alloys the reader is referred to ref.[131,175] Up-to-date results concerning the hot-deformation behavior of high Nb containing TiAl alloys and β-stabilized TiAl alloys, including processing maps, can be found in ref.[12,17,68,102,106,112,176–181] Consistently, all authors state that in TiAl alloys which contain high amounts of Nb, Mo, W, or other β-stabilizing elements dynamic recrystallization and globularization of the microstructure is retarded. These effects are attributed to strain localization in shear bands and a generally lower diffusibility. Moreover, due to the high

  

ADVANCED ENGINEERING MATERIALS



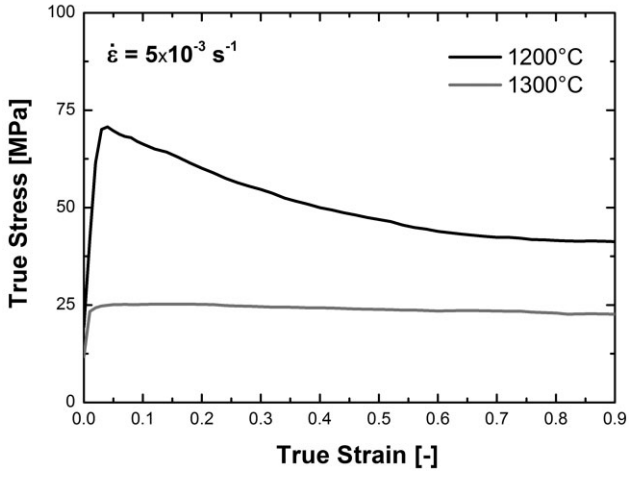


*Fig. 17. Flow curves of a cast and HIPed TNM alloy obtained in compression at 1200 and 1300 °C applying a deformation rate of $5 \times 10^{-3}$ s$^{-1}$.[168] The starting microstructure is shown in Figure 16b.*

volume fraction of readily deformable β-phase, the amount of strain energy imparted into the $\alpha/\alpha_2$- and γ-phases is comparably small so that the driving force for dynamic recrystallization in these constituents is reduced. As a consequence the restoration of the microstructure in the β-phase is far in advance of that of the α- and γ-phase as proposed by Appel *et al*.[12,87]

Figure 18a shows the microstructure of a TNM alloy after forging under isothermal conditions, while Figure 18b–c display the microstructure after hot-die forging, followed by relatively fast cooling to room temperature. Whereas isothermal forging is conducted at a rather low deformation rate,[9,12,17] the strain rates employed in the hot-die process are significantly higher[28,29] and increase from Figure 18b–d (in the following qualitatively assigned to ''slow,'' ''medium,'' and ''fast''). From Figure 18a it is obvious that during isothermal forging dynamic recrystallization and globularization have occurred and a refinement of the starting microstructure (see Figure 16b) has taken place. Note the lamellar colonies lying in the plane of the forging already existed in the casting and were not deformed during hot-working. Figure 18b shows the microstructure after ''slow'' hot-die forging. Obviously, during forging the β-phase has aligned perpendicularly to the forging direction and also the former α-grains show an elongated feature. Note that the formation of the lamellar $\gamma/\alpha_2$-colonies took place after the forging process during cooling to room temperature. In addition, characteristic features of dynamic recrystallization can be seen, i.e., areas which consist of fine globular grains forming a so-called necklace structure at the boundaries of former α-grains. An increase in both temperature and deformation rate lead to microstructures depicted in Figure 18c and d. Both microstructures exhibit elongated grains, but the formation of fine-grained areas, as presented in Figure 18b, was suppressed. Evidently, fast forging and subsequent fast cooling, which are characteristics of the hot-die process, lead to a significant amount of stored deformation energy in the material which can be utilized in following heat treatments.[163,182]

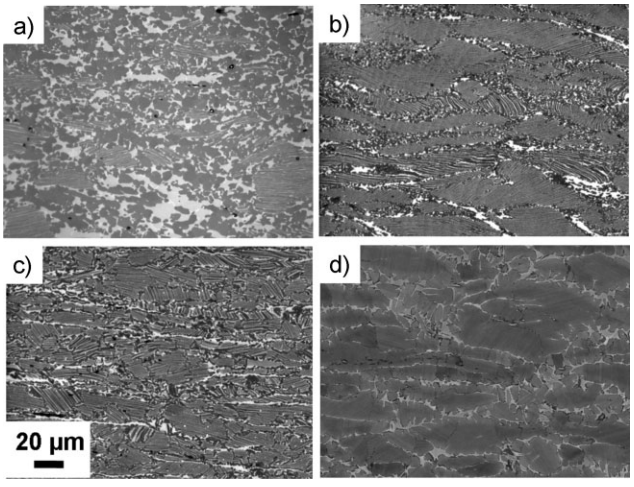


*Fig. 18. Microstructure of a Ti–43.5Al–4Nb–1Mo–0.1B alloy after (a) isothermal forging; (b) hot-die forging (''slow''); (c) hot-die forging (''medium''); (d) hot-die forging (''fast''). Due to confidentiality no specific information of the forging parameters can be given. SEM images taken in BSE mode. Forging direction is vertically.*

In order to study the hot-working behavior of TNM alloys in real time, in situ HEXRD experiments were conducted during hot-compression tests in the $(\alpha + \beta)$ phase field.[30,32] A novel technique was employed to evaluate the diffraction data with respect to the microstructural processes occurring during deformation.[31] Additional electron back-scatter diffraction (EBSD) investigations have been carried out allowing to distinguish between the mechanisms of recovery and recrystallization as reported in ref.[31,32] It has been found that in the disordered β-phase, as a consequence of the high stacking fault energy of the bcc lattice, fast dynamic recovery is maintaining a low defect density during deformation. On the contrary, dislocation activity increases the defect density in the α-phase which is counterbalanced to some extent by a relatively slow recovery process. In some regions, the dislocation density might increase to such an extent that recrystallization occurs in the α-phase.[32] However, hot-deformation within the three-phase field region $(\alpha + \beta + \gamma)$ is accompanied by a significant share of dynamic recrystallization leading to a refinement of the microstructure.[32,163,182] In the end, the results derived from the in situ studies confirm the assumption of Appel *et al*.[87] on the deformation and refining mechanisms which occur during hot-working of high β-phase containing TiAl alloys.

Koeppe *et al*.[183] conducted extensive quantitative microstructural and fracture surface analysis on forged Ti–48Al–2Cr specimens which were tested at room temperature under four-point bending conditions. They pointed out, that the plastic fracture strain of equiaxed microstructures is mainly governed by the homogeneity of the microstructure (Figure 19a) rather than by grain size or composition effects. For example, coarse microstructural defects which are embedded in an otherwise fine-grained matrix lead to an increased grain size ratio $d_c/d_m$ [= coarse grain size ($d_c$)/mean

  

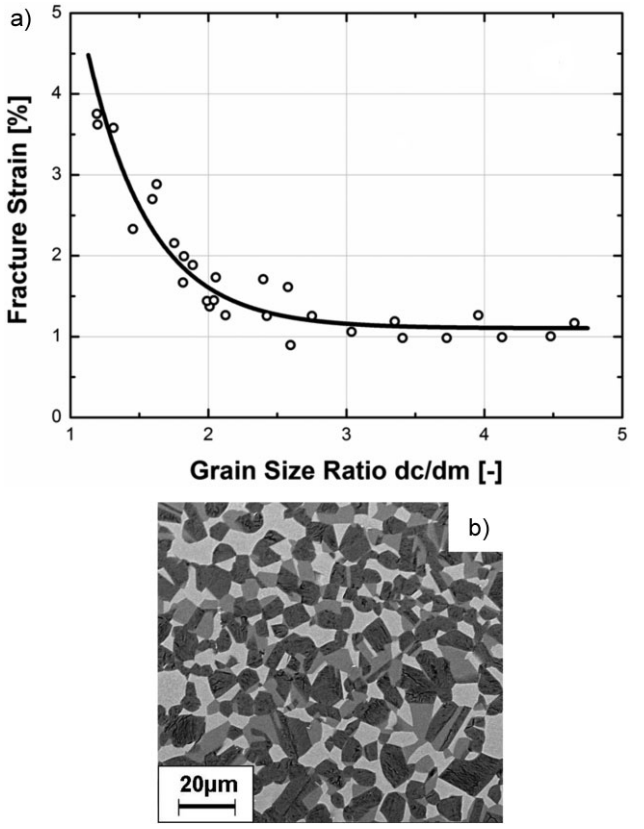


*Fig. 19. (a) Dependence of the bending fracture strain of Ti–48Al–2Cr on the grain size ratio $d_c/d_m$ [= coarse grain size ($d_c$)/mean grain size ($d_m$)] according to Koeppe et al.,[183] (b) microstructure of a Ti–43.5Al–4Nb–1Mo–0.1B alloy which was subjected to a special heat treatment to increase the microstructural quality after the hot-die forging process (Figure 17). SEM image taken in BSE mode.[182,184]*

grain size ($d_m$); see Figure 19a] and, consequently, a decrease of the plastic fracture elongation is caused due to premature crack initiation. In forged β-stabilized TiAl alloys, such microstructural inhomogeneities might be elongated $\beta_o$- and $\alpha_2$-grains as well as residual lamellar colonies (Figure 18). The relationship between microstructure and fracture elongation as shown in Figure 19a has a great practical importance for the microstructural design of TiAl components where a certain – and reproducible – fracture elongation below the brittle-to-ductile temperature is demanded. In order to structurally homogenize the forged microstructure shown in Figure 18b–d, a heat treatment was developed which utilizes both the stored deformation energy and thermodynamic non-equilibrium present after the forging process.[98,182] Figure 19b shows a representative image of a heat-treated hot-die forging which clearly proves the increase in microstructural homogeneity. Such a microstructure offers a good starting point for a further heat treatment which then determines the mechanical properties of the fabricated component.

In order to realize microstructures which provide balanced mechanical properties, a two-step heat treatment has been developed for TNM alloys which are thoroughly reported in ref.[28,184] After the first heat treatment step, conducted in the $(\alpha+\beta+\gamma)$-phase field region followed by AC, the microstructure consists of a small volume fraction of globular $\beta_o$- and γ-grains as well as supersaturated $\alpha_2$-grains with a grain size well below 100 µm. The second heat treatment step, which in fact is an ageing treatment within the $(\alpha_2+\beta_o+\gamma)$-phase field region, has a strong effect on the mechanical properties because ultra-fine lamellar $\gamma/\alpha_2$-colonies are formed by decomposition of the supersaturated $\alpha_2$-grains. In situ TEM and HEXRD experiments, e.g., see ref.[185] were carried out to study nucleation and precipitation of very fine γ-lamellae from supersaturated $\alpha_2$-grains during the second heat treatment step. The mean interface spacing, including $\alpha_2/\gamma$- and γ/γ-interfaces, is in the range of 15–30 nm and depends primarily on the temperature at which the second heat treatment is performed. The ageing conditions, e.g., temperature and time duration, must be selected in such a way that cellular reactions are avoided which lead to a break-up of the lamellar colonies and consequently to a refinement of the microstructure.[28,162,163] The microstructural investigations have been conducted by SEM, TEM, and HRTEM. Exemplarily, Figure 20 shows the nearly lamellar microstructure after the described two-step heat treatment. These TEM investigations revealed the presence of ω-phase within the $\beta_o$-grains. Since ω possesses a $B8_2$ structure it exhibits lower symmetry than the $\beta_o$-phase and the formation might affect the material's ductility. The average size of the ω-domains was determined to be in the range of 150–300 nm, depending on the ageing parameters.[28,162]

Figure 20 shows clearly that the heat-treated microstructure is dominated by lamellar $\gamma/\alpha_2$-colonies. From literature it is well established that the mechanical properties of γ-TiAl based alloys are often determined by the presence of a (nearly) lamellar microstructure which can be substantially varied by modifying the spacing between the internal $\alpha_2$-$Ti_3Al$/γ-TiAl

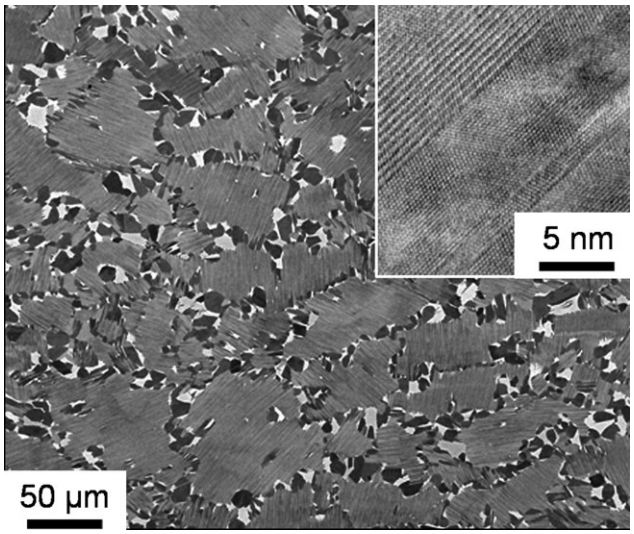


*Fig. 20. Nearly lamellar microstructure of a Ti–43Al–4Nb–1Mo–0.1B alloy after a two-step heat treatment. The majority of the microstructure consists of lamellar γ/$\alpha_2$-colonies with globular γ-grains (dark contrast) and $\beta_o$-grains (bright contrast) at their boundaries and triple points (SEM-BSE image). The inset shows a HRTEM image of a γ/$\alpha_2$-colony.[182]*

  

ADVANCED ENGINEERING MATERIALS



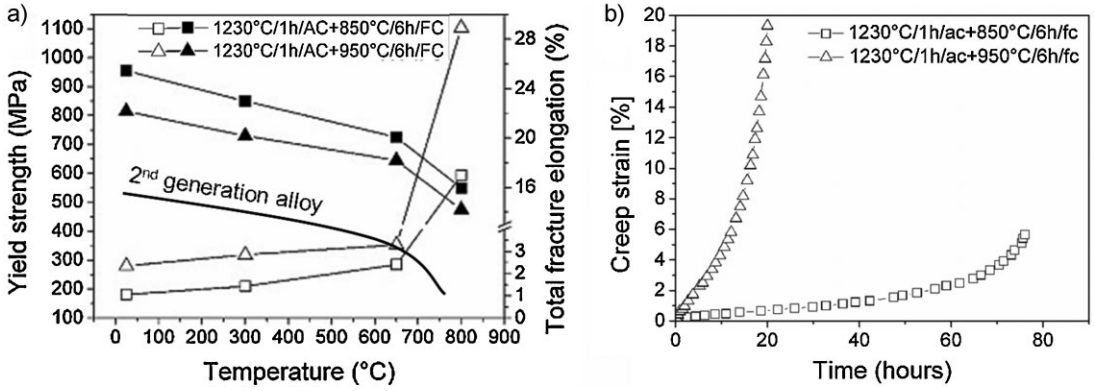


*Fig. 21. (a) 0.2%-yield strength (■,▲) and total fracture elongation (□,Δ) for two different ageing temperatures.[28] The investigated nearly lamellar microstructure is shown in Figure 20. Specimens aged at 850 °C for 6 h exhibit an average interface spacing of 13 nm, whereas the samples aged at 950 °C possess a spacing of 27 nm. The volume fraction of globular γ- and $\beta_o$-grains was kept constant. For comparison the yield strength of a typical 2nd generation TiAl alloy is indicated;[20] (b) Results of creep tests conducted in air at 800 °C and 300 MPa. The relatively high creep stress of 300 MPa was selected to discern the effect of the difference in lamellar spacing within short test times.*

hetero-phase as well as γ-TiAl/γ-TiAl homo-phase boundaries.[2,12,42,47] The observed behavior of the yield strength (Figure 21a) can be explained by a modified Hall–Petch relationship where the dominant structural parameter is the mean interface spacing. The stress required to propagate dislocations through the interfaces is inversely proportional to the square root of the mean interface spacing.[11,186] Here, the $\gamma/\alpha_2$- and γ/γ-interfaces act as glide obstacles and lead to dislocation pile-ups as observed by TEM investigations.[47] The plastic fracture elongation of TNM alloys at ambient temperatures depends critically on the volume fraction of the globular γ- and $\beta_o$-grains which are arranged around the lamellar $\alpha_2/\gamma$-colonies, because $\beta_o$-phase tends to embrittle the material, whereas γ-phase increases the ductility. Additionally, the average lamellar spacing and thus the volume fraction of γ-phase within the colonies contributes to the overall deformation behavior (Figure 21a).

Numerous investigations have revealed that also the creep behavior of lamellar γ-TiAl based alloys is strongly dependent on the mean interface spacing.[187–191] The creep behavior shown in Figure 21b is in accordance with this finding and shows that a decreasing mean interface spacing leads to a decreasing creep strain and creep rate ($\dot{\varepsilon}$). However, a steady state creep rate becomes barely discernable when $\dot{\varepsilon}$ versus $\varepsilon$ is plotted, which is a common feature of TiAl alloys, regardless of the prevailing microstructure.[47] Consequently, the minimum creep rate is used for the determination of the stress exponent $n$ and the activation energy of creep $Q$. The minimum creep rate can be described as a power law function with the mean interface spacing as a parameter.[192] Two mechanisms can account for the observed strong dependence of the creep behavior on the mean interface spacing. The first mechanism is based on the assumption that dislocation glide and climb is impeded by a reduced interface spacing.[193,194] The second mechanism proposes that the dislocation motion is restricted parallel to the $\alpha_2/\gamma$-interfaces causing a bowing out of dislocation segments between the interfaces.[47,195,196] The creep resistance of γ-TiAl based alloys which contain high additions of Nb, Mo, W, and other refractory metals is generally higher when compared to that of 2nd generation alloys with similar microstructures. This behavior is attributed to the reduction of diffusivity, abating diffusion-assisted climb processes which are the rate controlling mechanism during creep deformation.[11,12] Additionally, doping with C can also lead to a significant improvement of the creep strength (see Section 2). In case of β-stabilized TiAl alloys, such as TNM alloys, the volume fraction of the $\beta_o$-phase present at application temperature must be controlled carefully in order to avoid a deterioration of the creep properties.[87] The stress exponent of a TNM alloy with a nearly lamellar microstructure related to that shown in Figure 20 was determined to be $n \approx 3$ for a test temperature of 750 °C and a stress range of 150–250 MPa. The corresponding activation energy for creep is about 370 kJ mol$^{-1}$,[137] which agrees well with the result derived from internal friction measurements.[197] As in case of the tensile properties the creep resistance of TNM alloys depends on the arrangements of the constituent phases within the microstructure. As mentioned above the presence of lamellar $\alpha_2/\gamma$-colonies increases the creep strength, in which the lamellar spacing plays a decisive role. The existence of globular γ-TiAl grains, which is a controlling factor as far as room temperature ductility is concerned, decreases the creep strength and thus the volume fraction must be chosen carefully.[28]

More specific information concerning microstructure evolution and mechanical properties of advanced TiAl alloys, including fatigue and fracture behavior, can be found in ref.[4,7–9,12,198]

## 5. Applications in Automotive and Aircraft Engines

World-wide the demand for reduced fuel consumption, emissions, and noise in motor vehicles is steadily increasing. For example, regulations which will limit emissions from mid- to large size diesel engines will soon be enforced in Europe and the USA. The European automotive industry is meeting this challenge by further downsizing their conventional

  

combustion engines. Additionally, efficiency and engine performance will be enhanced by increasing combustion gas temperatures up to 850 °C (diesel engine) and 1050 °C (gasoline engine) where gas pressures and engine revolutions per minute are simultaneously rising. As a consequence, the requirements for oscillating and rotating components operating at high temperatures are steadily increasing as reported in ref.[2,10,12,14–18,199,200] Thus, new light-weight, high temperature materials and cost-effective production techniques must be developed and applied. In this context, γ-TiAl based alloys exhibit a promising combination of low density and high strength at elevated temperatures.

According to Baur *et al*.[14] with the use of light-weight TiAl alloys for turbocharger wheels the following benefits are expected to occur. First of all, a reduction of emissions, especially soot, as a result of the quicker charging of fresh air for the combustion process. An improvement of the response behavior (''turbo-lag''), as shown in Figure 22b, increases the agility of the vehicle's responsiveness. An appreciable reduction of noise and vibration is caused by the shift of the resonance frequencies to higher levels. Furthermore, the foundations are laid for an increase in the maximum rpm of the turbine rotor, and consequently, the turbocharger and engine efficiency. An additional beneficial effect of the lower rotor mass is a lower necessary protection against busting of the turbine wheel, which leads to lower housing wall thicknesses. Moreover, bearing friction is reduced and thus the whole turbocharger system can achieve higher efficiency and longer durability. Figure 22a shows a TiAl turbocharger wheel used for car engine tests and Figure 22b shows one of the derived test results. Although the test data are confidentially and, thus, the numbers on the diagram are omitted, the impact of TiAl is clearly recognizable.[14] In 1999, the first commercial application of γ-TiAl based alloys was announced. Mitsubishi has implemented TiAl turbocharger wheels in their Lancer Evolution 6 sports car.[18] The turbine wheels were produced by means of the LEVICAST process, a modification of the lost wax precision casting method, as well as by centrifugal casting. Researchers of DAIDO in cooperation with universities have developed advanced TiAl alloys which contain high additions of Nb to improve the high-temperature properties and other alloying elements to ensure good castability.[17] In addition, time and effort were spent to establish sound manufacturing routes which, e.g., includes joining of the TiAl wheel to the steel shaft, e.g., see ref.[18,201] It should be noted that in Europe ABB has equipped the two diesel engines of an operational high-speed ferry with γ-TiAl turbocharger wheels. This ferry has been in successful operation with the TiAl wheels for over 2 years, for a total of over 4000 h service time.[202] However, it must be critically noted that at present the use of TiAl alloys is restricted to diesel engines. In order to implement this innovative class of materials in gasoline engines further alloy development is required to improve both creep strength and oxidation resistance. Engine valves appear to be another suitable application for γ-TiAl based alloys.[1–3,7] In 2002, the commercial production of wrought processed high-performance γ-TiAl valves for racing car application has started.[10,38] The processing route is a variant of multi-step extrusion. Further production steps include precision machining and coating.

The next generation of aircraft engines is targeted to exhibit higher efficiency which leads to reduced kerosene consumption, significant lower emission of $CO_2$ and $NO_x$ as well as to a noticeable reduction of engine noise. Until 2020, according to the guidelines set by the Advisory Council for Aeronautics Research in Europe (ACARE), emission of $CO_2$ and $NO_x$ and engine noise should be reduced by 50, 80, and 50%, respectively, taking the current status of technology as reference value (www.acare4europe.org.). Such ambitious targets can only be realized by applying improved engine design concepts in combination with the use of advanced materials. There are at least three major payoff areas for γ-TiAl based alloys in advanced aero engines:[2,4,7,10,15,20–22] (a) γ-TiAl has a specific elastic stiffness 50% greater than structural materials commonly used in aircraft engines (Figure 1b). The higher specific stiffness ($E/\rho$) also shifts acoustically excited vibrations toward higher frequencies, which is usually beneficial for structural components, e.g., compressor and turbine blades and parts within the exhaust nozzle area. (b) The good creep resistance of advanced γ-TiAl based alloys in the temperature regime of 600–800 °C enables the substitution of heavy Ni-based alloys for certain applications. (c) The high fire resistance of γ-TiAl based alloys (nearly as resistant as Ni-based alloys) can enable the substitution of heavy and expensive fire-resistant designed Ti-based alloys in some components. Only few years ago, General Electric announced the initiation of investment cast blades of a 2nd generation TiAl alloy in the LPT[13] because this section of the engine offers the highest weight reduction potential. Since then certification and flight tests with TiAl equipped engines have been conducted

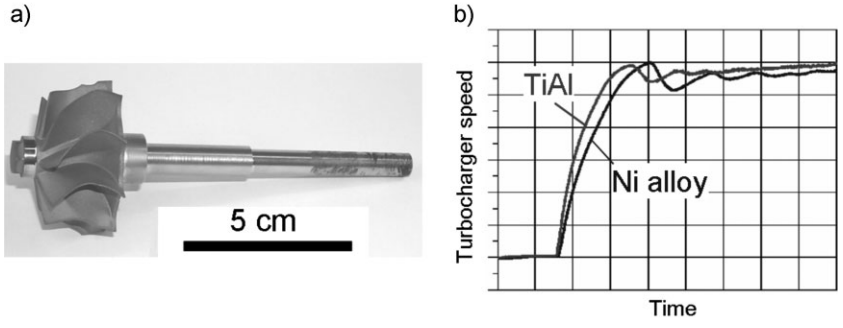


*Fig. 22. (a) Turbine rotor with a TiAl wheel used for a diesel engine. The turbocharger wheel was produced by means of gravity casting. After HIPing the wheel was connected to the shaft by high-temperature brazing and subsequently machined and balanced; (b) result of a vehicle test with a car equipped with a TiAl turbocharger (XD45 alloy) and a conventional Ni-based turbocharger. For more information see ref.[14]*

  

ADVANCED ENGINEERING MATERIALS



successfully and in the meantime the regular service for carriage of freight and passenger transport has begun already.[203] Meanwhile also other major aero engine manufacturers have announced in press releases and their homepages the future use of TiAl in their next jet engine generation. Depending on engine type 100 to 150 LPT blades per stage are required.[204] Advanced engine concepts as reported in ref.,[15,203,205,206] however, involve higher mechanical loading of the LPT blades, thus demanding the use of high-strength advanced γ-TiAl based alloys.

## 6. Conclusions

Intermetallic γ-TiAl based alloys are considered as a very important candidate material for advanced applications in aerospace, automotive, and related industries. World-wide research and development on γ-TiAl alloys have led to a better understanding of the fundamental influence of alloy composition and microstructure on mechanical properties and processing behavior. During the last years industry has started to use this new class of light-weight high-temperature materials. In particular, all major aircraft and automotive engine manufacturers are advancing the qualification and introduction of γ-TiAl components. Engineering γ-TiAl based alloys can be processed using advanced metallurgical methods – a factor, which is decisive for these specific materials to be economically competitive with other state-of-the-art materials. In current γ-TiAl based alloys balanced properties like room temperature ductility, fracture toughness, high-temperature strength, creep, and oxidation resistance can be achieved. In order to further extend the use of these innovative intermetallic materials more applications in automotive and aero engines as well as other areas must be identified. To this end, future research shall be directed to further increase the high-temperature capabilities of TiAl alloys as well as to develop smart coating concept which guarantee safe protection and lifetime of a component. Concurrently, reliable and cost-effective production routes have to be established.

*Received: July 3, 2012*
*Final Version: October 9, 2012*
*Published online: November 19, 2012*

[1] Y.-W. Kim, D. M. Dimiduk, M. H. Loretto (Eds), *Gamma Titanium Aluminides 1999*, TMS, Warrendale, PA, USA **1999**.
[2] H. Clemens, H. Kestler, *Adv. Eng. Mater.* **2000**, *9*, 551.
[3] K. J. Hemker, D. M. Dimiduk, H. Clemens, R. Darolia, H. Iui, J. M. Larson, V. K. Sikka, M. Thomas, J. D. Whittenberger (Eds), *Structural Intermetallics, 2001*, TMS, Warrendale, PA, USA **2001**.
[4] Y.-W. Kim, H. Clemens, A. H. Rosenberger (Eds), *Gamma Titanium Aluminides 2003*, TMS, Warrendale, PA, USA **2003**.
[5] M. J. Mills, H. Inui, H. Clemens, C.-F. Fu (Eds), *Integrative Interdisciplinary Aspects of Intermetallics*, Materials Research Society, Symp. Proc., Vol. *842*, Pittsburgh, PA, USA **2005**.
[6] J. Wiezorek, C.-L. Fu, M. Takeyama, D. Morris, H. Clemens (Eds), *Advanced Intermetallics-Based Alloys*, Materials Research Society, Symp. Proc., Vol. *980*, Pittsburgh, PA, USA **2007**.
[7] Y.-W. Kim, D. Morris, R. Yang, C. Leyens (Eds), *Structural Aluminides for Elevated Temperature Applications*, TMS, Warrendale, PA **2008**.
[8] M. Palm, B. P. Bewlay, K. S. Kumar, K. Yoshimi (Eds), *Intermetallic-Based Alloys for Structural Functional Applications*, Materials Research Society, Symp. Proc., Vol. *1295*, Pittsburgh, PA, USA **2011**.
[9] C. Leyens, M. Peters (Eds), *Titanium Titanium Alloys*, WILEY-VCH, Weinheim **2003**.
[10] H. Clemens, W. Smarsly, *Adv. Mater. Res.* **2011**, *278*, 551.
[11] F. Appel, M. Oehring, R. Wagner, *Intermetallics* **2000**, *8*, 1283.
[12] F. Appel, J. D. H. Paul, M. Oehring, in *Gamma Titanium Aluminide Alloys – Science and Technology*, WILEY-VCH, Weinheim **2011**.
[13] B. P. Bewlay, in *Presentation at the ''European Symposium on Superalloys and their Applications''*, Wildbad Kreuth, Germany, May 25–28, **2010**
[14] H. Baur, D. B. Wortberg, H. Clemens, in *Gamma Titanium Aluminides 2003* (Eds: Y.-W. Kim, H. Clemens, A. H. Rosenberger), TMS, Warrendale, PA, USA **2003**, p. 23.
[15] W. Smarsly, H. Baur, G. Glitz, H. Clemens, T. Khan, M. Thomas, in *Structural Intermetallics 2001*, The Minerals, Metals And Materials Society, TMS, Warrendale, PA, USA **2001**, p. 25.
[16] T. Tetsui, in *Gamma Titanium Aluminides 1999* (Eds: Y.-W. Kim, D. M. Dimiduk, M. H. Loretto), TMS, Warrendale, PA **1999**, p. 15.
[17] T. Noda, *Intermetallics* **1998**, *6*, 709.
[18] T. Tetsui, *Adv. Eng. Mater.* **2001**, *3*, 307.
[19] F. Appel, U. Brossmann, U. Christoph, S. Eggert, P. Janschek, U. Lorenz, J. Müllauer, M. Oehring, J. D. H. Paul, *Adv. Eng. Mater.* **2000**, *11*, 699.
[20] E. A. Loria, *Intermetallics* **2000**, *8*, 1339.
[21] X. Wu, *Intermetallics* **2006**, *14*, 1114.
[22] A. Lasalmonie, *Intermetallics* **2006**, *14*, 1123.
[23] H. Kestler, H. Clemens, in *Titanium and Titanium Alloys* (Eds: C. Leyens, M. Peters), WILEY-VCH, Weinheim **2003**, p. 351.
[24] D. M. Dimiduk, *Mater. Sci. Eng. A* **1999**, *263*, 281.
[25] H. F. Chladil, H. Clemens, A. Otto, V. Güther, S. Kremmer, A. Bartels, R. Gerling, *Berg- und Hüttenmännische Monatshefte (BHM)* **2006**, *151*, 356.
[26] H. Clemens, W. Wallgram, S. Kremmer, V. Güther, A. Otto, A. Bartels, *Adv. Eng. Mater.* **2008**, *10*, 707.
[27] M. Schloffer, F. Iqbal, H. Gabrisch, E. Schwaighofer, F.-P. Schimansky, S. Mayer, A. Stark, T. Lippmann,

  

M. Göken, F. Pyczak, H. Clemens, *Intermetallics* **2012**, *22*, 231.
[28] W. Wallgram, T. Schmoelzer, L. Cha, G. Das, V. Güther, H. Clemens, *Int. J. Mater. Res.* **2009**, *100*, 1021.
[29] S. Kremmer, H. Chladil, H. Clemens, A. Otto, V. Güther, in *Ti-2007 Science and Technology*, The Japan Institute Of Metals (JIM), Sendai, Japan **2008**, p. 989.
[30] T. Schmoelzer, K.-D. Liss, P. Staron, S. Mayer, H. Clemens, *Adv. Eng. Mater.* **2011**, *13*, 685.
[31] K. Liss, T. Schmoelzer, K. Yan, M. Reid, M. Peel, R. Dippenaar, H. Clemens, *J. Appl. Phys.* **2009**, *106*, 113526.
[32] T. Schmoelzer, K.-D. Liss, C. Kirchlechner, S. Mayer, A. Stark, M. Peel, H. Clemens, *Intermetallics* **2012**, submitted.
[33] K. Liss, A. Bartels, A. Schreyer, H. Clemens, *Textures Microstruct.* **2010**, *35*, 219.
[34] K. D. Liss, A. Bartels, H. Clemens, S. Bystrzanowski, A. Stark, T. Buslaps, F. P. Schimansky, R. Gerling, C. Scheu, A. Schreyer, *Acta Mater.* **2006**, *54*, 3721.
[35] S. Kabra, K. Yan, S. Mayer, T. Schmoelzer, M. Reid, R. Dippenaar, H. Clemens, K.-D. Liss, *Int. J. Mater. Res. (formerly Z. Metallkd.)* **2011**, *102*, 697.
[36] T. Schmoelzer, K.-D. Liss, G. A. Zickler, I. J. Watson, L. M. Droessler, W. Wallgram, T. Buslaps, A. Studer, H. Clemens, *Intermetallics* **2010**, *18*, 1544.
[37] I. J. Watson, K.-D. Liss, H. Clemens, W. Wallgram, T. Schmoelzer, T. C. Hansen, M. Reid, *Adv. Eng. Mater.* **2009**, *11*, 932.
[38] Information on. http://www.mwracing.eu.
[39] M. Weimer, *paper presented at the ''4th International Workshop on Titanium Aluminides,'' Nuremberg, Germany (September 14–16, 2011).*
[40] Y.-W. Kim, *J. Met.* **1989**, *41*, 24.
[41] S. C. Huang, J. C. Chessnut, in *Intermetallic Compounds – Principles and Practice*, Vol. 2 (Eds: J. H. Westbrook, R. L. Fleischer), Wiley & Sons, West Sussex, UK **1994**, p. 73.
[42] Y. Kim, *J. Met.* **1994**, *46*, 30.
[43] Y.-W. Kim, D. M. Dimiduk, *J. Met.* **1991**, *43*, 40.
[44] H. Clemens, A. Lorich, N. Eberhardt, W. Glatz, W. Knabl, H. Kestler, *Z. Metallkd.* **1999**, *90*, 569.
[45] S. C. Huang, E. L. Hall, *Metall. Trans.* **1991**, *22A*, 427.
[46] Y.-W. Kim, *Mater. Sci. Eng.* **1995**, *A 192/193*, 519.
[47] F. Appel, R. Wagner, *Mater. Sci. Eng.* **1998**, *R22*, 187.
[48] F. Kauffmann, T. Bidlingmaier, G. Dehm, A. Wanner, H. Clemens, *Intermetallics* **2000**, *8*, 823.
[49] W. T. Marketz, F. D. Fischer, F. Kauffmann, G. Dehm, T. Bidlingmaier, A. Wanner, H. Clemens, *Mater. Sci. Eng. A* **2002**, *329–331C*, 177.
[50] W. T. Marketz, F. D. Fischer, H. Clemens, *Int. J. Plast.* **2003**, *19*, 281.
[51] F. D. Fischer, F. Appel, H. Clemens, *Acta Mater.* **2003**, *51*, 1249.
[52] H. Petryk, F. D. Fischer, W. Marketz, H. Clemens, F. Appel, *Metall. Mater. Trans. A* **2003**, *34A*, 2827.
[53] F. Appel, F. D. Fischer, H. Clemens, *Acta Mater.* **2007**, *55*, 4915.
[54] F. D. Fischer, T. Waitz, C. Scheu, L. Cha, G. Dehm, T. Antretter, H. Clemens, *Intermetallics* **2010**, *18*, 509.
[55] R. Pippan, F. Wetcher, M. Hafok, A. Vorhauer, I. Sabirov, *Adv. Eng. Mater.* **2006**, *8*, 1046.
[56] E. M. Eidenberger, *Diploma Thesis*, Montanuniversitaet Leoben, Austria **2012**.
[57] C. Mangler, C. Gammer, H. P. Karnthaler, C. Rentenberger, *Acta Mater.* **2010**, *58*, 563.
[58] M. Takeyama, Y. Kato, M. Kikuchi, in *Titanium 95* (Eds: P. A. Blekinsop, W. J. Evans, H. M. Flower), The Institute of Materials, London, England **1996**, p. 294.
[59] M. Takeyama, M. Kikuchi, *Mater. Jpn.* **1996**, *35*, 1058.
[60] A. Suzuki, M. Takeyama, T. Matsuo, *Intermetallics* **2002**, *10*, 915.
[61] R. Kainuma, Y. Fujita, H. Mitsui, I. Ohnuma, K. Ishida, *Intermetallics* **2000**, *8*, 855.
[62] H. Nakamura, M. Takeyama, W. Kin, Y. Yamabe, M. Kikuchi, in *SAMPE Symposium on Intermetallic Compounds for High-Temperature Structural Applications* (Eds: M. Yamaguchi, H. Fukutomi), Society for the Advancement of Materials and Process Engineering, Chiba, Japan **1993**, p. 997.
[63] R. M. Imayev, V. M. Imayev, M. Oehring, F. Appel, *Intermetallics* **2007**, *15*, 451.
[64] V. Küstner, M. Oehring, A. Chatterjee, V. Güther, H.-G. Brokmeier, H. Clemens, in *Gamma Titanium Aluminides 2003* (Eds: Y.-W. Kim, H. Clemens, A. H. Rosenberger), TMS, Warrendale, PA, USA **2003**, p. 89.
[65] H.-G. Brokmeier, M. Oehring, U. Lorenz, H. Clemens, F. Appel, *Metall. Trans. A* **2004**, *35*, 3563.
[66] A. Bartels, H. Kestler, H. Clemens, *Mater. Sci. Eng. A* **2002**, *329–331C*, 152.
[67] W. Schillinger, A. Bartels, R. Gerling, F.-P. Schimansky, H. Clemens, *Intermetallics* **2006**, *14*, 336.
[68] A. Stark, A. Bartels, H. Clemens, S. Kremmer, F.-P. Schimansky, R. Gerling, *Adv. Eng. Mater.* **2009**, *11*, 976.
[69] H. Clemens, H. F. Chladil, W. Wallgram, G. A. Zickler, R. Gerling, K.-D. Liss, S. Kremmer, V. Güther, W. Smarsly, *Intermetallics* **2008**, *16*, 827.
[70] M. Yamaguchi, H. Inui, K. Ito, *Acta Mater.* **2000**, *48*, 307.
[71] D. R. Johnson, K. Chihara, H. Inui, M. Yamaguchi, *Acta Mater.* **1998**, *18*, 6529.
[72] G. L. Chen, W. J. Zhang, Z. C. Liu, S. J. Li, Y.-W. Kim, in *Gamma Titanium Aluminides 1999* (Eds: Y.-W. Kim, D. M. Dimiduk, M. H. Loretto), TMS, Warrendale, PA, USA **1999**, 371.
[73] H. F. Chladil, H. Clemens, G. A. Zickler, M. Takeyama, E. Kozeschnik, A. Bartels, T. Bulaps, R. Gerling, S. Kremmer, L. Yeoh, K.-D. Liss, *Int. J. Mater. Res. (formerly Z. Metallkd.)* **2007**, *98*, 1131.
[74] C. Woodward, J. M. MacLaren, D. M. Dimiduk, in *High-temperature Ordered Intermetallic Alloys V*, Vol.

  

*288*, Mater. Res. Soc. Proc. (Eds: R. Darolia, J. D. Whittenberger, M. H. Yoo), Materials Research Society, Pittsburgh, PA, USA **1993**, p. 171.

[75] W. J. Zhang, F. Appel, *Mater. Sci. Eng. A* **2002**, *334*, 59.

[76] Y. Yuan, H. W. Liu, X. N. Zhoa, X. K. Meng, Z. G. Liu, T. Boll, T. Al-Kassab, *Phys. Lett. A* **2006**, *358*, 231.

[77] C. Herzig, T. Przeorski, M. Friesel, F. Hirsker, S. Divinski, *Intermetallics* **2001**, *9*, 461.

[78] Y. Mishin, Chr. Herzig, *Acta Metall.* **2000**, *48*, 589.

[79] C. Leyens, in *Titanium and Titanium Alloys* (Eds: C. Leyens, M. Peters), WILEY-VCH, Weinheim **2003**, p. 187.

[80] D. Gosslar, R. Günther, U. Hecht, C. Harting, R. Bormann, *Acta Mater.* **2010**, *58*, 6744.

[81] W. J. Zhang, S. C. Deevi, *Mater. Sci. Eng.* **2003**, *A337*, 17.

[82] H. S. Park, S. W. Nam, N. J. Kim, S. K. Hwang, *Scr. Mater.* **1999**, *41*, 1197.

[83] L. Cha, C. Scheu, H. Clemens, H. Chladil, G. Dehm, R. Gerling, A. Bartels, *Intermetallics* **2008**, *16*, 868.

[84] Y. Chen, F. Kong, J. Han, Z. Chen, J. Tian, *Intermetallics* **2005**, *13*, 263.

[85] W. Li, B. Inkson, Z. Horita, K. Xia, *Intermetallics* **2000**, *8*, 519.

[86] T. T. Cheng, M. R. Willis, I. P. Jones, *Intermetallics* **1999**, *7*, 89.

[87] F. Appel, J. D. H. Paul, M. Oehring, H. Clemens, F. D. Fischer, *Z. Metallkd.* **2004**, *95*, 585.

[88] R. Gerling, F.-P. Schimansky, A. Stark, A. Bartels, H. Kestler, L. Cha, C. Scheu, H. Clemens, *Intermetallics* **2008**, *16*, 689.

[89] C. Scheu, E. Stergar, M. Schober, L. Cha, H. Clemens, A. Bartels, F.-P. Schimansky, A. Cerezo, *Acta Mater.* **2009**, *57*, 1504.

[90] F. Appel, J. D. H. Paul, M. Oehring, U. Fröbl, U. Lorenz, *Metall. Mater. Trans. A* **2003**, *34*, 2149.

[91] W. H. Tian, M. Nemato, *Intermetallics* **1997**, *5*, 237.

[92] F. Perdrix, M.-F. Trichet, J.-L. Bonnentien, M. Cornet, J. Bigot, *Intermetallics* **2001**, *9*, 807.

[93] A. Menand, A. Huguet, A. Nérac-Partaix, *Acta Mater.* **1996**, *44*, 4729.

[94] J. Rossouw, C. T. Forwood, M. A. Gibson, P. R. Miller, *Philos. Mag. A* **1996**, *74*, 77.

[95] Y. Song, R. Yang, D. Li, Z. Q. Hu, Z. X. Guo, *Intermetallics* **2000**, *8*, 563.

[96] A. Denquin, S. Naka, A. Huguet, A. Menand, *Scr. Mater.* **1993**, *28*, 1131.

[97] H. Gabrisch, A. Stark, F.-P. Schimansky, L. Wang, N. Schell, U. Lorenz, F. Pyczak, *Intermetallics* **2012**, submitted.

[98] M. Schloffer, E. Schwaighofer, H. Clemens, S. Mayer, *Research under progress, unpublished results* **2012**.

[99] D. Zhang, P. Kopold, V. Güther, H. Clemens, *Z. Metallkd.* **2000**, *91*, 206.

[100] D. Zhang, G. Dehm, H. Clemens, *Scr. Mater.* **2000**, *42*, 1065.

[101] D. Zhang, G. Dehm, H. Clemens, *Z. Metallkd.* **2000**, *91*, 950.

[102] H. Y. Kim, W. H. Sohn, S. H. Hong, *Mater. Sci. Eng. A* **1998**, *251*, 216.

[103] Y. Jin, J. N. Wang, J. Jang, Y. Wang, *Scr. Mater.* **2004**, *51*, 113.

[104] W. G. Burgers, *Physica* **1934**, *1*, 561.

[105] C. McCullough, J. J. Valencia, G. G. Levi, R. Mehrabian, *Acta Metall.* **1989**, *37*, 1321.

[106] T. Tetsui, K. Shindo, S. Kobayashi, M. Takeyama, *Scr. Mater.* **2002**, *47*, 399.

[107] T. Tetsui, K. Shindo, S. Kobayashi, M. Takeyama, *Intermetallics* **2003**, *11*, 299.

[108] T. Tetsui, K. Shindo, S. Kaji, S. Kobayashi, M. Takeyama, *Intermetallics* **2005**, *13*, 971.

[109] F. Appel, M. Oehring, J. D. H. Paul, *Adv. Eng. Mater.* **2006**, *8*, 371.

[110] T. T. Cheng, M. H. Loretto, *Acta Mater.* **1998**, *46*, 4801.

[111] Y. H. Wang, J. P. Lin, Y. H. He, Y. L. Wang, G. L. Chen, *Mater. Sci. Eng. A* **2007**, *471*, 82.

[112] H. Z. Niu, Y. Y. Chen, S. L. Xiao, F. T. Kong, C. J. Chang, *Intermetallics* **2011**, *19*, 1767.

[113] Z. W. Huang, W. Voice, P. Bowen, *Scr. Mater.* **2003**, *48*, 79.

[114] N. Saunders, in *Gamma Titanium Aluminides 1999* (Eds: Y.-W. Kim, D. M. Dimiduk, M. H. Loretto), TMS, Warrendale, PA **1999**, p. 183.

[115] I. Ansara, *Int. Metall. Rev.* **1979**, *22*, 20.

[116] N. Saunders, A. P. Miodownik, in *CALPHAD: A Comprehensive Guide*, Pergamon Materials Series, Vol. 1 (Ed: R. W. Cahn), Pergamon, Oxford **1998**.

[117] H. Chladil, H. Clemens, H. Leitner, A. Bartels, R. Gerling, F.-P. Schimansky, S. Kremmer, *Intermetallics* **2006**, *14*, 1194.

[118] V. T. Witusiewicz, A. A. Bondar, U. Hecht, T. Y. Velikanova, *J. Alloys Compd.* **2009**, *472*, 89.

[119] V. T. Witusiewicz, A. A. Bondar, U. Hecht, S. Rex, T. Y. Velikanova, *J. Alloys Compd.* **2008**, *465*, 64.

[120] Y. Liu, E. Gamsjäger, H. Clemens, *Int. J. Mater. Res. (formerly Z. Metallkd.)* **2011**, *102*, 692.

[121] Z. Zhang, K. J. Leonard, D. M. Dimiduk, V. K. Vasudevan, in *Structural Intermetallics 2001*, (K. J. Hemker, D. M. Dimiduk, H. Clemens, R. Darolia, H. Inui, J. M. Larsen, V. K. Sikka, M. Thomas, J. D. Whittenberger), TMS, Warrendale, PA **2001**, p. 515.

[122] Y.-W. Kim, D. M. Dimiduk, in *Structural Intermetallics 2001* (K. J. Hemker, D. M. Dimiduk, H. Clemens, R. Darolia, H. Inui, J. M. Larsen, V. K. Sikka, M. Thomas, J. D. Whittenberger), TMS, Warrendale, PA **2001**, p. 625.

[123] U. Hecht, V. Witusiewicz, A. Drevermann, J. Zollinger, *Intermetallics* **2008**, *16*, 969.

[124] M. Takeyama, S. Kobayashi, *Intermetallics* **2005**, *13*, 989.

[125] F. S. Sun, C. X. Cao, S. E. Kim, Y. T. Lee, M. G. Yan, *Metall. Mater. Trans. A* **2001**, *32*, 1573.

  

[126] D. R. Johnson, H. Inui, S. Muto, Y. Omiya, T. Yamanaka, *Acta Mater.* **2006**, *54*, 1077.
[127] R. Gerling, H. Clemens, F. P. Schimansky, *Adv. Eng. Mater.* **2004**, *6*, 23.
[128] M. Schloffer, T. Schmoelzer, S. Mayer, E. Schwaighofer, G. Hawranek, F.-P. Schimansky, F. Pyczak, H. Clemens, *Prakt. Metallogr.* **2011**, *48*, 594.
[129] M. Schloffer, E. Schwaighofer, A. Themeßl, H. Clemens, F. Heutling, D. Helm, M. Achtermann, S. Mayer, *paper presented at the ''4th International Workshop on Titanium Aluminides'', Nuremberg, Germany (September 14–16, 2011).*
[130] R. Werner, M. Schloffer, E. Schwaighofer, H. Clemens, S. Mayer, *Intermetallics*, Mater. Res. Symp. Proc., Symposium JJ, 2012 MRS Fall Meeting, submitted.
[131] F. Appel, H. Kestler, H. Clemens, in *Intermetallic Compounds – Principles and Practice*, Vol. 3, Progress (Eds: J. H. Westbrook, R. L. Fleischer), John Wiley Publishers, Chicester, UK **2002**, p. 617.
[132] F. Preli, J. Eßlinger, *paper presented at the ''4th International Workshop on Titanium Aluminides'', Nuremberg, Germany (September 14–16, 2011).*
[133] T. Schaden, F. D. Fischer, H. Clemens, F. Appel, A. Bartels, *Adv. Eng. Mater.* **2006**, *8*, 1109.
[134] A. Bartels, W. Schillinger, G. Graßl, H. Clemens, in *Gamma Titanium Aluminides 2003* (Eds: Y.-W. Kim, H. Clemens, A. H. Rosenberger), TMS, Warrendale, PA, USA **2003**, p. 275.
[135] N. Rizzi, *presentation at the Symposium ''Structural Aluminides for Elevated Temperature Applications'', TMS 2008 Annual Meeting, New Orleans, LA, USA (March 9–13, 2008).*
[136] D. Huber, in *Bohler Schmiedetechnik*, Kapfenberg, Austria, unpublished results **2012**.
[137] A. Gaitzenauer, M. Müller, H. Clemens, R. Hempel, P. Voigt, S. Mayer, *Berg- und Hüttenmännische Monatshefte (BHM)* **2012**, *157*, 319.
[138] V. Güther, A. Otto, J. Klose, C. Rothe, H. Clemens, W. Kachler, S. Winter, S. Kremmer, in *Structural Aluminides for Elevated Temperature Applications* (Eds: Y.-W. Kim, D. Morris, R. Yang, C. Leyens), TMS, Warrendale, PA **2008**, p. 249.
[139] J. R. Wood, in *Gamma Titanium Aluminides 2003* (Eds: Y.-W. Kim, H. Clemens, A. H. Rosenberger), TMS, Warrendale, PA, USA **2003**, p. 227.
[140] M. Achtermann, V. Güther, J. Klose, H.-P. Nicolei, *paper presented at the ''4th International Workshop on Titanium Aluminides'', Nuremberg, Germany (September 14–16, 2011).*
[141] J. Reitz, C. Lochbichler, B. Friedrich, *Intermetallics* **2011**, *19*, 762.
[142] R. Pippan, P. Hageneder, W. Knabl, H. Clemens, T. Hebesberger, B. Tabernig, *Intermetallics* **2001**, *9*, 89.
[143] K. S. Chan, D. S. Shih, *Metall. Trans.* **1998**, *29A*, 73.
[144] J. D. Campbell, Jj. Kruzic, S. Lillibridge, K. F. Venkateswara Rao, R. O. Ritchie, *Scr. Mater.* **1997**, *37*, 707.
[145] M. Blackburn, in *The Science, Technology and Application of Titanium*, Pergamon Press Ltd, Oxford **1970**, p. 633.
[146] M. Takeyama, T. Kumagai, M. Nakamura, M. Kikuchi, in *Structural Intermetallics* (Eds: R. Darolia, J. J. Lewandowski, C. T. Liu, P. L. Martin, D. B. Miracle, M. V. Nathal), TMS, Warrendale, PA **1993**, p. 167.
[147] S. A. Jones, M. J. Kaufman, *Acta Mater.* **1993**, *41*, 387.
[148] D. M. Dimiduk, V. K. Vasudevan, in *Gamma Titanium Aluminides 1999* (Eds: Y.-W. Kim, D. M. Dimiduk, M. H. Loretto), TMS, Warrendale, PA, USA **1999**, p. 239.
[149] R. Schnitzer, H. F. Chladil, C. Scheu, H. Clemens, S. Bystrzanowski, A. Bartels, S. Kremmer, *Pract. Metallogr.* **2007**, *44*, 430.
[150] H. I. Aaronson, V. K. Vasudevan, *Metall. Trans.* **2002**, *22A*, 2445.
[151] S. K. Bhattacharyya, J. H. Perepezko, T. B. Massalski, *Acta Mater.* **1974**, *22*, 879.
[152] H. Clemens, A. Bartels, S. Bystrzanowski, H. Chladil, H. Leitner, G. Dehm, R. Gerling, F.-P. Schimansky, *Intermetallics* **2006**, *14*, 1380.
[153] C. Scheu, L. Cha, S. Sturm, H. F. Chladil, P. H. Mayrhofer, H. Clemens, A. Bartels, W. Wolf, R. Podloucky, *Mater. Res. Symp. Proc.* **2007**, *980*, 0980-II05-01.
[154] D. Hu, X. Wu, M. H. Loretto, *Intermetallics* **2005**, *13*, 914.
[155] Y. Q. Sun, *Metall. Trans.* **1998**, *29A*, 2679.
[156] S. R. Dey, A. Hazotte, E. Bouzy, S. Naka, *Acta Mater.* **2005**, *53*, 3783.
[157] S. R. Dey, A. Hazotte, E. Bouzy, *Intermetallics* **2009**, *17*, 1052.
[158] D. Hu, A. J. Huang, X. Wu, *Intermetallics* **2005**, *13*, 211.
[159] M. Beschliesser, H. Clemens, H. Kestler, F. Jeglitsch, *Scr. Mater.* **2003**, *47*, 284.
[160] F. Appel, M. Oehring, D. H. Paul, *Adv. Eng. Mater.* **2006**, *8*, 371.
[161] A. Stark, A. Bartels, H. Clemens, F.-P. Schimansky, *Adv. Eng. Mater.* **2008**, *10*, 929.
[162] L. Cha, H. Clemens, G. Dehm, *Int. J. Mater. Res.* **2011**, *102*, 703.
[163] H. Clemens, S. Mayer, in *Ti-2011* (Eds: L. Zhou, H. Chang, Y. Lu, D. Xu), Science Press, Beijing, China **2012**, p. 395.
[164] T. Schmoelzer, A. Stark, E. Schwaighofer, T. Lippmann, S. Mayer, H. Clemens, *Adv. Eng. Mater.* **2012**, *14*, 445.
[165] B. J. Inkson, H. Clemens, J. Marien, *Scr. Mater.* **1998**, *38*, 1377.
[166] E. Schwaighofer, M. Schloffer, T. Schmölzer, S. Mayer, J. Lindemann, V. Güther, J. Klose, H. Clemens, *Pract. Metallogr.* **2012**, *49*, 3.
[167] M. Thomas, *Mater. Res. Soc. Symp. Proc.* **2011**, *1295*, 127.

  

[168] J. Lindemann, unpublished data, *BTU Cottbus*, Cottbus, Germany **2011**.
[169] F. J. Humphreys, M. Hatherly, in *Recrystallization and Related Annealing Phenomena*, Pergamon, Oxford **1995**, p. 364.
[170] Z. Deng, J. Li, T. Zhang, H. Zhong, R. Hu, H. Chang, in *Ti-2011* (Eds: L. Zhou, H. Chang, Y. Lu, D. Xu), Science Press, Beijing, China **2012**, p. 1486.
[171] S. L. Semiatin, V. Seetharaman, *Metall. Trans.* **1995**, *26A*, 371.
[172] S. L. Semiatin, V. Seetharaman, I. Weiss, *Mater. Sci. Eng.* **1998**, *A243*, 1.
[173] S. L. Semiatin, in *Gamma Titanium Aluminides* (Eds: Y-. W. Kim, R. Wagner, M. Yamaguchi), TMS, Warrendale, PA **1995**, p. 509.
[174] S. L. Semiatin, V. Seetharaman, I. Weiss, *Metall. Trans.* **1994**, *A25*, 2539.
[175] V. Seetharaman, S. L. Semiatin, *Metall. Trans.* **1996**, *27A*, 1987.
[176] W.-J. Zhang, U. Lorenz, F. Appel, *Acta Mater.* **2000**, *48*, 2803.
[177] T. Tetsui, *Intermetallics* **2002**, *10*, 239.
[178] J. D. H. Paul, F. Appel, R. Wagner, *Acta Mater.* **1998**, *46*, 1075.
[179] S. Li, X. Su, Y. Han, X. Xu, G. Chen, *Intermetallics* **2005**, *13*, 323.
[180] X. J. Xu, J. P. Lin, Y. L. Wang, J. F. Gao, Z. Lin, G. L. Chen, *J. Alloys Compd.* **2006**, *414*, 175.
[181] B. Liu, Y. Liu, Y. P. Li, W. Zhang, A. Chiba, *Intermetallics* **2011**, *19*, 1184.
[182] H. Clemens, T. Schmoelzer, M. Schloffer, E. Schwaighofer, S. Mayer, G. Dehm, *Mater. Res. Soc. Symp.* **2011**, *1295*, 95.
[183] C. Koeppe, A. Bartels, J. Seeger, H. Mecking, *Metall. Trans.* **1993**, *24A*, 1795.
[184] H. Clemens, S. Mayer, *Pract. Metallogr.* **2011**, *48*, 64.
[185] L. Cha, T. Schmoelzer, Z. Zhang, S. Mayer, H. Clemens, P. Staron, G. Dehm, *Adv. Eng. Mater.* **2012**, *14*, 299.
[186] G. Cao, L. Fu, J. Lin, Y. Zhang, C. Chen, *Intermetallics* **2000**, *8*, 647.
[187] G. Dehm, C. Motz, C. Scheu, H. Clemens, P. Mayrhofer, C. Mitterer, *Adv. Eng. Mater.* **2006**, *8*, 1033.
[188] P. D. Crofts, P. Bowen, I. P. Jones, *Scr. Mater.* **1996**, *35*, 1391.
[189] K. Maruyama, R. Yamamoto, H. Nakakuki, N. Fujitsun, *Mater. Sci. Eng. A* **1997**, *419*, 239.
[190] T. A. Parthasarathy, M. Keller, M. G. Mendiratta, *Scr. Mater.* **1998**, *37*, 1025.
[191] W. R. Chen, J. Triantafillou, J. Beddoes, L. Zhao, *Intermetallics* **1999**, *7*, 171.
[192] A. Chatterjee, H. Clemens, H. Mecking, G. Dehm, E. Arzt, *Z. Metallkd.* **2001**, *92*, 1000.
[193] R. W. Hayes, P. A. McQuay, *Scr. Mater.* **1994**, *30*, 259.
[194] B. D. Worth, W. Jones, J. E. Allison, *Metall. Mater. Trans. A* **1995**, *26*, 2947.
[195] J. Beddeos, W. Wallace, L. Zhao, *Int. Mater. Rev.* **1995**, *40*, 197.
[196] J. N. Wang, A. J. Schwartz, T. G. Nieh, C. T. Liu, V. K. Sikka, D. Clemens, in *Gamma Titanium Aluminides* (Eds: Y.-W. Kim, R. Wagner, M. Yamaguchi), TMS, Warrendale, PA, USA **1995**, p. 949.
[197] P. Simas, T. Schmoelzer, M. L. No, H. Clemens, J. S. Juan, *Mater. Res. Soc. Symp.* **2011**, *1295*, 139.
[198] W. F. Cui, C. M. Liu, V. Bauer, H.-J. Christ, *Intermetallics* **2007**, *15*, 675.
[199] T. Tetsui, S. Ono, *Intermetallics* **1999**, *7*, 689.
[200] Si.-Y. Sung Y.-J. Kim, *Intermetallics* **2006**, *14*, 1163.
[201] T. Tetsui, *Intermetallics* **2001**, *9*, 253.
[202] P. A. McQuay, in *Structural Intermetalics 2001* (Eds: K. J. Hemker, D. M. Dimiduk, H. Clemens, R. Darolia, H. Iui, J. M. Larson, V. K. Sikka, M. Thomas, J. D. Whittenberger), TMS, Warrendale, PA, USA **2001**, p. 83.
[203] M. Weimer, B. Bewlay, T. Schubert, *paper presented at the ''4th International Workshop on Titanium Aluminides'', Nuremberg, Germany (September 14–16, 2011).*
[204] J. Aguliar, O. Kättlitz, T. Stoyanov, *paper presented at the 4th European Conference on Materials and Structures in Aerospace, Hamburg, Germany, (February 7–8, 2012).*
[205] R. Martens, *VDI Nachrichten*, June 17, 2011.
[206] G. Das, W. Smarsly, F. Heutling, C. Kunze, D. Helm, *paper presented at the ''4th International Workshop on Titanium Aluminides'', Nuremberg, Germany (September 14–16, 2011).*

  